REPUBLIC OF TURKEY
BİNGÖL UNIVERSITY
INSTITUTE OF SCIENCE

PREPARATION OF Ni DOPED Cu_2O MATERIALS VIA ELECTROCHEMICAL DEPOSITION METHOD AND ITS PHOTOELECTROCATALYTIC APPLICATION

MASTER'S THESIS

NASHMEEL HAMAD ALI

CHEMISTRY

THESIS ADVISOR
Prof. Dr. İBRAHİM Y. ERDOĞAN

BİNGÖL-2018

REPUBLIC OF TURKEY
BİNGÖL UNIVERSITY
INSTITUTE OF SCIENCE

PREPARATION OF Ni DOPED Cu_2O MATERIALS VIA ELECTROCHEMICAL DEPOSITION METHOD AND ITS PHOTOELECTROCATALYTIC APPLICATION

MASTER'S THESIS

Nashmeel Hamad ALI

Department : CHEMISTRY

This dissertation was accepted by the following committee on 03.01.2018 with the vote unity.

Prof. Dr.	**Assoc. Prof. Dr.**	**Prof. Dr.**
Ramazan SOLMAZ	**Mehmet KAHRAMAN**	**İbrahim Y. ERDOĞAN**
Head of examining committee	**Member of examining committee**	**Member of examining committee**

I confirm the result above

Prof. Dr. İbrahim Y. ERDOĞAN

Director of the institute

PREFACE

First and foremost I wish to express my sincere gratitude and thanks to god for giving me this great opportunity to pursue my master degree in which I gained successfully and for blessing me and helping me in my life.

I would particularly like to thank my supervisor Prof. Dr. İbrahim Y. ERDOĞAN without his help and commitment to my work this thesis would have been vastly more difficult to complete.

I would like to express my deepest appreciation to Chemistry Department and Central Laboratory staff and to all those who provide me the possibility to complete this research.

I appreciate the support of my friend assistant researcher Barzan MIRZA, so I am also thankful for my husband who allow me and supported me with his responsibility during my study. I would like to express my deep gratitude to all members my family especially my sister Narmin HAMAD for the encourage and support during my study finally thanks to all my friends who supported me in this period my study.

Dedication

For my lovely mother and my son Halan BOTAN

Nashmeel Hamad ALI

Bingöl 2018

CONTENTS

LIST OF SYMBOLS AND ABBREVIATIONS

A	: Ampere
Å	: Angstrom
CA	: Chronoamperometry
cm^2	: Centimeters meter square
CV	: Cyclic voltammetry
CVD	: Chemical vapor deposition:
d	: Distance
E	: Electrode potential
E	: Standard electrode potential
ED	: Electrodeposition
EDX	: Energy dispersive X-ray spectroscopy
Eg	: Band gap
eV	: Electron volts
FETs	: Field-effect transistors
g	: Gram
Ipa	: Anodic peak current
Ipc	: Cathodic peak current
K	: Kelvin
kj	: Kilojoule
L	: Litter
Log	: Logarithm
LSV	: Linear sweep voltammetry
mA	: Miliamper
mAh	: Miliamper/hour
mm	: Milimeter
mL	: Mililitter
mV	: Milivolt

μm	: Micrometer
n	: Number of electron
nm	: Nanometer
NPs	: Nanoparticles
Pa	: Pascal
PEC	: Photoelectrochemistry
ppm	: Parts per million
s	: Second
Sccm	: Standard cubic centimeter-minute
SEM	: Scanning electron microscopy
T	: Temperature
t	: Time
UPD	: Underpotential deposition
UV-Vis	: Ultraviolet visible
XRD	: X-ray diffraction
V	: Volt
Ω	: Electrical resistance
λ	: Wavelength

LIST OF FIGURES

ELEKTROKİMYASAL DEPOZİSYON YÖNTEMİ İLE Ni KATKILI Cu_2O MALZEMELERİNİN HAZIRLANMASI VE FOTOELEKTROTOKATALİTİK UYGULAMASI

ÖZET

Bu tez çalışması, Cu_2O yarıiletken malzemelerin fotoelektrokimyasal özelliklerine nikel katkılama miktarının etkisi üzerine sistematik bir çalışmadır. Katkısız Cu_2O yarıiletken malzemeleri elektrokimyasal yöntem kullanılarak hazırlandı. Doğrusal taramalı voltametri (LSV) tekniği nikeli katkılamak için kullanıldı. Malzemelerin karakterizasyonu enerji dağılımlı X-ışını spektroskopisi (EDX), taramalı elektron mikroskopu (SEM), X-ışını kırınımı (XRD), morötesi-görünür bölge (UV-Vis) spektroskopisi, LSV ve kronoamperometri (CA) teknikleri kullanılarak gerçekleştirildi. EDX spektrumları, materyallerin içerdiği elementler hakkında detaylar sağladı ve numunelerde bulunan elementlerin sayısal analizini ortaya koydu. Sonuçlar Ni katkılı Cu_2O malzemelerinin varlığını gösterir. Tüm SEM görüntülerinde, elektronun yüzeyine yaklaşık olarak aynı boyutta eşit olarak dağılan kristaller gözlendi. Çoğu Cu_2O ve Ni katkılı Cu_2O kristal malzeme tek tip biçime sahiptir. XRD sonuçları ITO substrat üzerine biriktirilen Ni katkılı Cu_2O malzemelerinin yüksek kristal yapıya sahip olduğunu gösterir. Malzemelerin bant aralığı enerjisinin Eg = 2,14 eV olduğu belirlendi. Tüm fotoelektrokimyasal ölçümler, Ni katkılı Cu_2O malzemelerinin p-tipi doğasına bağlı olarak fotokatodik davranış gösterdi. Bu çalışma, 0,0002 M $NiSO_4$ çözeltisi kullanarak Ni katkılanan Cu_2O fotoelektrotların incelenen tüm Ni katkılı Cu_2O fotoelektrotlar arasında en yüksek fotoakım ve akım yoğunluğu sergilediğini gösterdi. Katkısız Cu_2O ve Ni katkılı Cu_2O fotoelektrotlar farklı nikel katkılama miktarları için iyi bir kararlılık davranışı gösterdi. Ni katkılı Cu_2O yarıiletken fotoelektrotları, ileri fotoelektrokimyasal dedeksiyon, fotoelektrokimya su ayrıştırma ve diğer solar fotovoltaik teknolojilerin geniş bir alanı için rekabetçi bir aday olarak önerilebilir.

Anahtar Kelimeler: Ni katkılı Cu_2O, elektrokimyasal depozisyon, Ni katkılama etkisi, fotoelektrot.

PREPARATION OF Ni DOPED Cu_2O MATERIALS VIA ELECTROCHEMICAL DEPOSITION METHOD AND ITS PHOTOELECTROCATALYTIC APPLICATION

ABSTRACT

This thesis study reports on a systematic study of the influence of the amount of nickel doping on the photoelectrochemical characteristics of Cu_2O semiconductor materials. Undoped Cu_2O semiconductor materials were prepared by the electrochemical method. Linear sweep voltammetry (LSV) technique was used to dope nickel. Characterization of the materials was performed by energy dispersive X-ray spectroscopy (EDX), scanning electron microscopy (SEM), X-ray diffraction (XRD), ultraviolet–visible (UV–Vis) spectroscopy, LSV and chronoamperometry (CA) techniques. The EDX spectra provided details about the elements present in the materials and present the numerical analysis of the elements present in the samples. The results indicate presence of Ni doped Cu_2O materials. In all SEM images, evenly distributed the crystals of approximately the same size are observed on the surface of the electrode. Most Cu_2O and Ni doped Cu_2O crystalline materials have a uniform shape. XRD results indicate that Ni doped Cu_2O materials deposited over ITO substrate have highly crystalline structure. The band gap energy of the materials was found to be Eg = 2.14 eV. All the photoelectrochemical measurements showed a photocathodic behavior due to the p-type nature of the Ni doped Cu_2O materials. This work showed that the Cu_2O photoelectrodes doped with Ni using 0.0002 M $NiSO_4$ solution exhibit the highest photocurrents and the current density between the investigated all Ni doped Cu_2O photoelectrodes. The undoped Cu_2O and Ni doped Cu_2O photoelectrodes exhibited a good stability behavior for different the amounts of nickel doping. Ni doped Cu_2O semiconductor photoelectrodes are suggested as a competitive candidate for advanced photoelectrochemical detection, maybe for the extended field of photoelectrochemical water splitting and other solar photovoltaic technologies.

Keywords: Ni doped Cu_2O, electrochemical deposition, effect of doping Ni, photoelectrode.

1. INTRODUCTION

1.1. Semiconductors

Semiconductor is the basic building blocks of all modern electronic device and able to conduct or block electrical current, in order to this ability of semiconductor serve a significant function in every things from relays to the integrate circuits of computer. Semiconductors consist of materials whose electronic properties are intermediate among those of metals and insulators (Schroder 2006). These characteristics are determined by the structure of the bonding characteristics, electronic energy bands, crystal, and also by the fact that unlike metals, in which semiconductor has both the positive (hole) and the negative (electron) electricity carriers which whose densities controlled during the crystal growth by doping the pure semiconductor with chemical impurities. In classification solids according their electrical properties, that indicated there are two types (metals and semiconductors) materials.

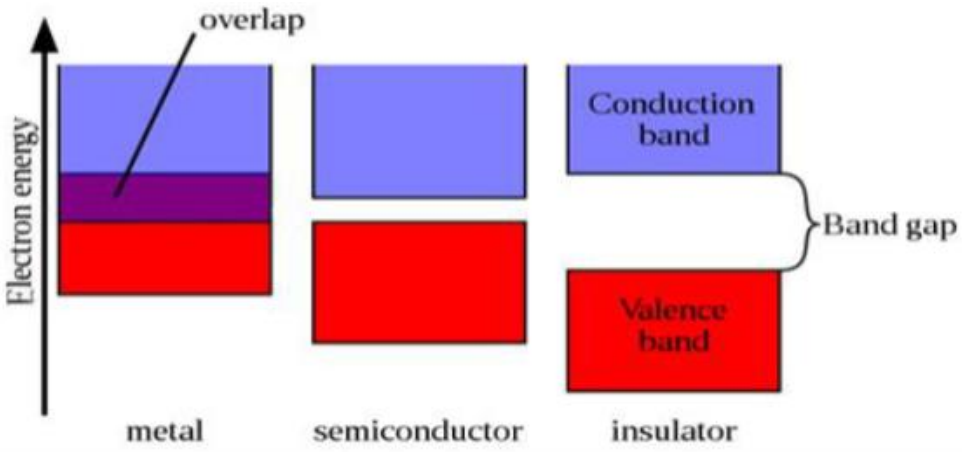

Figure 1.1. The band gap in semiconductors, insulators, and the overlap in metals

The metals have permanent electron gases permeating the total of the solid and are limited within the solid. The insulators are materials with reality no free electrons moving, unable electrical conductivity in order to there is no electron gas (Pillai 2010).

Normally the energy band gap in semiconductors is in the range of 1-4 eV. The band gap width is determines the conductivity of the material with its optical response. In opposite to semiconductors, metals are characterized by a high density of electronic states at energies just above the Fermi level (Memming 2001). In which at the Fermi level electrons can be thermally excited into these empty states cause the high electrical conductivity of metals, high excitation energies in intrinsic semiconductors are necessary to overcome the band gap and to rise electrons from the valence band to the conduction band leaving behind electron holes. Both positive and negative charge carriers can contribute to the electrical conductivity. In the case of extrinsic semiconductors, the carriers charge number depends on the concentration of dopant in the material. The introduction of acceptor or donor species of electrons in the semiconductor can alter perceptibly its electronic structure and consequently its Fermi level. Usually, doping is carried out by the introduction of atoms with a higher or a lower number of valence electrons, giving rise to an n-type or p-type semiconductor, respectively. Consequently, majority charge carriers are electrons in the first case and holes in the second case (Soga et al. 2006).

At recent time, best positional and orientation control was completed as well as the demonstration of the first pn-junctions based on hetero structured nanowhiskers. This was followed by significant studies in two separate research laboratories in the mid-1990s. A new whisker growth mechanism was proposed by William Buhro's group at Washington University, where they manufactured III-V nanowhiskers using a solution-liquid-solid process (Yang et al. 2010). Meanwhile, Charles Lieber group at Harvard initiated a research program in the area of inorganic nanorods. Carbide and oxide nanorods were formed through vapor phase exchange and transport processes in some of these early studies. These recent works on nano whiskers and nanorods were popularized as semiconductor nanowires in the following decade. In the late 1990s, the field of semiconductor nanowires underwent a significant expansion and became one of the most active research areas within the nano science community (Xia et al. 2003).

1.2. Methods of Producing Semiconductors

There are more efforts have been prepared for the fabrication and control of shape and size of semiconductor nanostructures, in the past few years, because of their importance in catalysis, photonics, electronics, sensing, optoelectronics, and utilize nano devices in potential applications (Alivisatos et al. 2005). The most significantly of semiconductor nano materials stems are length scale and, equally important, in which these properties change with their size or shape. This acquired from the fact to novel properties. There are more methods have been developed to fabricate semiconductor nanostructures (Kumar and Nann 2006), for instance wet-chemical methods, including solvo thermal/hydrothermal method (Yu et al. 1998) and capping agent/surfactant assisted soft synthesis approach (Aldana et al. 2005), sonochemical methods (Zhu et al. 2003), templating methods (Xu et al. 2005), selfassembly oriented attachment growth (Tang et al. 2002), chemical vapor deposition (CVD) method (Jiang et al. 2003), electrochemical deposition methods (Erdoğan and Demir 2011). On the other hand, hybrid structures compose of semiconducting organic slabs and powerfully luminescent semiconductor nanostructures offer favorable perspectives through highly saturated, tunable optical properties, in mixture with an easy process-ability from solution and low cost of precursors, which is of significance for high-tech applications such as hybrid inorganic–organic light-emitting diodes and solar cells (Coe et al. 2002). In latest years, novel nanostructures of functional II-VI semiconductor chalcogenides, using thermal evaporation method by Wang's group and Lee's group in manufactured nanosaws, nanobelts, nanocombs, nanowires, and nano windmills (Moore et al. 2004 and Jiang et al. 2006).

1.3. Electrochemical Production Methods and Advantages

Electrochemical deposition is one of the most powerful methods for the production of thin films. It provides advantages such as the ability to synthesis at low temperature, high purity in the products and low costs. Also, electro deposition allows the thickness, stoichiometry, and microstructure of the films to be controlled by adjusting the deposition parameters. It can be prepared a various materials from this way (Georgieva et al. 2002). The advantages of this method for designing electrodes for lithium batteries are also well-

documented, particularly for tin alloy-based materials (Beattie et al. 2003). In which electrochemical deposition method was used to prepare Cu_2O films, which recently shown to react reversibly with Li (Laik et al. 2002), because the composition and microstructure of the films thus obtained is strongly affected by deposition variables, which explore the possibility of obtaining Cu_2O films of variable morphology over the same substrate simply by adjusting the deposition parameters. The structural and textural properties measured by X-ray diffraction (XRD), X-ray photoelectron spectroscopy (XPS), and scanning electron microscopy (SEM) measurements (Zhou et al. 1998).

Electrodeposition, which is widely used for metal or metallic alloys, for long time, appeared more later for semiconductors. Electrochemical reaction is a chemical reaction which occurs at the interface between two conductors which is electrode and electrolyte of an electrochemical cell system, due to the process of electron transfer between the electrolyte and the electrode. This is called a redox (reduction-oxidation) reaction. Oxidation reaction happens on the anode and the reduction reaction happens on the cathode (Wijesooriyage 2011). So electrochemical deposition is the most important electrochemical technique that uses to deposit of an element or a compound which is dissolved in the electrolyte as ions on top of an electrode by reduction reactions. The deposition of precious metals chemically treating or electrochemically (electrochemical deposition) has much more important role in the technologies life up to now where these metals are used. Exactly this is right in the scope of electrodeposition as this method depends on some different parameters such as temperature, pH and current density is likely to produce different kinds of deposit structures (Oku et al. 2014).

1.4. Photoelectrochemistry

The photoelectrochemistry of semiconductors (Pleskov et al. 1986) starts in the 19th century. It is problematic to estimate the first work of photoelectrochemistry, however, it appears that it was the work realized 170 years ago by Becquerel, in which found that an electric current is produced when a semiconductor electrode immersed into electrolytic solution is illuminated (Finn 1980). Several concepts that have served as a principal for the improvement photoelectrochemistry that related to the photoelectrochemical oxidized metals and behavior adsorbed layers (Ibl and Vogt 1981). The photoelectrochemistry of

semiconductors, as independent scientific branch, began in the 1950s, when Brattain and Garrett achieved to establish the relationship between the properties of photoelectrochemical monocrystalline semiconductors and their normal electronic structure. At the same time, this discipline began to utilize the basic of the classical theory of electrochemistry (Brattain and Garrett 1955).

A basis advance in the improvement of this discipline was constituted by the study of Gerischer (Gerischer and Lübke 1988). Photoelectrochemistry received a considerable impulse in 1970s when Fujishima and Honda confirmed water decomposition into oxygen and hydrogen under UV light illumination. Using a cell consisting of a semiconductor (TiO_2) and a metallic electrode (counter-electrode) immersed in an aqueous electrolyte, to generate chemical energy from used the light energy (Fujishima and Honda 1972). The fundamental studies to clarify the requirement of electron transfer through the semiconductor/electrolyte interface. Begging from the initial Gerischer model, various systems have been studied, such as dispersions of nanoparticles, quantum dots arrays, hybrid materials, nanocrystalline electrodes, etc. Besides, studies purpose at a systematic optimization of the physicochemical material properties guideline the photocatalytic process (Koval and Howard 1992).

It is essential to mention that photo electrochemistry proportionally related to heterogeneous photocatalysis in solution and extensively studied attributable to its more direct applications. In photocatalysis oxidation reactions take place (based on the transfer of photogenerated holes) and reduction reactions occur (involving photogenerated electrons) simultaneously. The overall reactions depend on a precise balance of these two processes (Castellar Ramos et al. 2012). In the situation of catalyst particles or particle agglomerates, while oxidation and reduction processes take place in parallel that balance is limited to discrete units with electron–hole recombination. Like photocatalyst particles then could be considered photoelectrochemical cells under short circuit situations (Bard 1979).

A major electrochemistry advantage used for the analysis and manipulation of photocatalytic reactions is based on the possibility of separating anodic and cathodic processes at different electrodes and of performing experiments under potentiostatic

control. This provides a very systematic and controlled technique of gaining fundamental knowledge on processes of relevance for the overall photocatalytic occurrence.

1.5. Copper

Cu is a 3d transition metal and has various interesting chemical and physical properties. Cu-based materials can rise and undergo a variety of reactions due to Cu's have wide range of accessible oxidation states (Cu, Cu (I), Cu (II), and Cu (III)), which enable reactivity via both one- and two-electron pathways. Because of their properties and unique characteristics, Cu-based nano catalysts have found various applications in nanotechnology, including electro catalysis, catalytic organic transformations, and photo catalysis (Ranu et al. 2012).

The main challenge in the development of catalytic nanoparticles (NPs) is to prepare nanomaterial's that are highly active, stable, robust, selective, and inexpensive (Aissa et al. 2015). In which nanomaterial's prepared from inexpensive and earth-abundant metals have attracted greatly attention because of their potential as practical alternatives to the rare and expensive noble-metal catalysts used in many normal commercial chemical processes. These metal NPs more demonstration activity dissimilar from that of the corresponding bulk materials because of their changed sizes and shapes, which give rise to distinctive quantum properties. In this context, Cu NPs are principally attractive because of copper's low cost, high natural abundance and the practical and straightforward multiple ways of preparing Cu-based nanomaterials (Zhang et al. 2006). Despite the strong background on the bulk Cu applications in various fields (e.g., optics, electronics, etc.), the use of Cu NPs is restricted by Cu's inherent instability under atmospheric conditions, which makes it prone to oxidation. Many efforts to develop the methods and supporting materials that increase the stability of Cu NPs by altering their sensitivity to oxygen, water, and other chemical entities has encouraged the exploration of alternative Cu-based NPs with more complex structures, such as core/shell Cu NPs or systems based on copper oxides.

1.6. Copper Oxide

In lastly years, copper-oxide-based materials have found applications in various areas such as heterogeneous catalysis (Li et al. 2008), gas sensing (Ishihara et al. 1998), superconducting (Chmaissem et al. 1999), and solar energy conversion (Minami et al. 2004). One economical way of generating advanced Cu-based nanomaterials for catalysis is to anchor Cu NPs (e.g., Cu, CuO, or Cu_2O) on supports such as SiO_2, iron oxides, carbon-based materials, or polymers. Additionally, Cu's high boiling point makes it compatible with high-temperature and pressure chemical reactions, including continuous flow reactions, vapor phase reactions, microwave-assisted reactions, and various organic transformations (Aissa et al. 2015). Such unique properties, conducive for the development of reactive and selective catalytic systems, have made Cu and its alloys between the most valuable metals in the past, and will warrant that they remain imperative in the future.

Copper oxides used in photoelectrochemical (PEC) for hydrogen production from solar-driven water splitting because they are nontoxic, abundant, and natively p-type also absorb visible light, although they face challenging issues such as instability in aqueous phases. In which copper oxides can be produced by different methods such as sputtering (Pierson et al. 2003), thermal evaporation (Huang et al. 2004), sonochemical methods (Kumar et al. 2001), thermal relaxation (Deki et al. 1998), and electrodeposition (Chatterjee et al. 1991). Between these methods, the electrochemical deposition was most powerful due to low-temperature growth process, can be highly cost effective and it provides controlled growth, which leads to preferred morphology, structure, also orientation that exact specific applications. For PEC applications, nanostructures such as nanowires and nanoparticles are often utilize as an approach to improve PEC performance due to the greatly increased surface areas (Ahn et al. 2008). It has been a challenge to grow copper oxide nanostructures on bare substrates. Typically, the growth of nanowires requires the use of a template and surfactants.

Also cupric oxide (CuO) is considered as one of the metal oxides with has great practical importance as a p-type semiconductor in electronics and optoelectronic devices; such as gas sensors (Katti et al. 2003)., nano fluid (Lee et al. 1999), high-TC super conductors

(Zheng et al. 2000), magnetic storage devices (Fan et al. 2003), catalysts (She et al. 2009) etc. Now a series of plans have been proved to manufacture nanoparticles CuO, such as colloid thermal synthesis (Son et al. 2009), solid state reaction (Wang et al. 2006), reflux condensation (Mageshwari et al. 2013), thermal decomposition of precursors (Salavati-Niasari and Davar 2009), sol-gel (Mallick and Sahu 2012), sonochemical (Vijaya Kumar et al. 2001) and hydrothermal (Zhang et al. 2006) etc.

1.7. Copper-I-Oxide (Cu_2O) Properties

Cu_2O nanoparticles, as a supper p-type semiconductor with have attracted considerable attention. And, Cu_2O nanoparticles have been widely used in different field's principle on their electronic, unique magnetic and optical properties. It is known that the sizes, structures and shapes which can effects the potential applications are dependent on the conditions of synthesis and methods (Lu et al. 2006). The synthesis methods of Cu_2O include long-chained alcohol reduction, electro-deposition, sol gel, solution phase and also chemical reduction (Zoolfakar et al. 2014). Some synthesis methods were more or less having some shortcomings. For instance, large quantities of organic matter being used in the long-chained alcohol reduction method are damaging to the environment and hard to handle, and also the method needs the condition of high temperature. The sol gel, solution phase are not possible for mass production. Therefore, the most frequently used method is the chemical reduction, reducing Cu (II) ions to Cu (I) ions, followed by the stabilization step for the Cu_2O nanoparticles in the solution (Wiley et al. 2004).

1.8. Nickel Properties

Nickel element is silvery-white color, hard, malleable, and ductile metal. It in the iron group from periodic table, it is an equally good electricity and heat conductor, bivalent familiar, although it assumes other valences (Andersen et al. 1997). Most nickel complexes compound are green or blue. Nickel dissolves slowly in dilute acids but, like iron, when treated with nitric acid becomes passive. Finely divided nickel adsorbs hydrogen. Nickel naturally rare exists in the environment (Diwan et al. 1992). Nickel is an essential element in most animal species, and it has been recommended it may be essential to human nutrition. Nickel is used for nickel alloys, batteries, electroplating,

industrial plumbing, coins, machinery parts, spark plugs, stainless-steel, nickel-chrome resistance wires, and catalysts. Nickel carbonyl has severely limited use in nickel refining (Barbour et al. 2009).

The great use of nickel is in the synthesis of alloys. Nickel alloys are characterized by ductility, strength, and resistance to heat and corrosion. Approximately 65 % of the nickel from the Western World consumed, used to make stainless steel, whose composition can vary but is normally iron with about 18% chromium and 8% nickel. Also 12 % of all the nickel spends into super alloys. The remaining 23% of consumption is divided among rechargeable batteries, alloy steels, catalysts and other coinage, chemicals, foundry plating and products (Chigane and Ishikawa1994). Nickel is easy to work, drawn into wire, resists corrosion even at high temperatures and in order to use in rocket engines and gas turbines. Nickel-copper alloy like Monel consist of (e.g. 70% nickel, 30% copper with traces of manganese, iron and silicon), which is not only hard but can resist corrosion by sea water, so that it is ideal for propeller shaft in desalination plants and boats (Paulonis et al. 1969).

Most Earth nickel is inaccessible because it is locked away in the planet's iron-nickel molten core, which is 10 % nickel. The total amount of nickel in the sea dissolved has been calculated to be around 8 billion tons. Oil and coal contain considerable amounts of nickel because organic matter has a strong ability to absorb the metal. The nickel content in some clay and loamy soils can be as high as 450 ppm or as low as 0.2 ppm in soil. The average is around 20 ppm (Wold et al. 1957). Nickel exists in some beans where it is an essential component of various enzymes. Additional relatively rich source of nickel is tea which has 7.6 mg/kg of dried leaves. Most ores from which nickel is extracted are iron-nickel sulphides, such as pentlandite (Cataldo et al. 1978).

1.9. Nickel Doping

Metal oxide nanostructured production and characterization of materials have been considered a keystone in modern materials science for both fundamental and technological reasons (Liang et al. 2014). Furthermore, studying their chemical and physical properties is of special interest, as compared to the bulk materials, because of

their widespread applications in various ranges (Humayun et al. 2013). Several transition metal oxides like Fe_3O_4, SnO_2, CuO revealed to be promising candidates for more applications. Production of bimetal oxide nanoparticles is a field of great interest between researchers due to its catalytic activity and transition metal doped synthesis with metal oxide nanoparticles becomes much more attention in current research (Stengl et al. 2011).

Moreover, semiconductor nanoparticles interest in doping with impurity metal ions is to explore the possibility of modifying electrical, optical and magnetic properties of the material. There were some researchers have reported the development in a material's characteristics by various dopants, in which addition of nickel to copper oxides improvement its strength, resistance to corrosion and also durability. The nickel doped copper oxide nanoparticles catalytic activity (Ni doped CuO NPs) is determined by many reasons such as time, temperature and preparation of catalyst (Sharma et al. 2014), also that the optical band gap increases from 3.9 eV to 4.3 eV with the increase in Ni content in CuO matrix (Basith et al. 2014). In which nickel doped copper oxide synthesized through hydrothermal method under controlled reaction temperature and pressure. The authors were able to achieve a variety of morphologies and particle sizes of NPs (Rahdar et al. 2014).

The dopants concentrations play major roles in the positions of emission bands and luminescence efficiency of semiconductor nanoparticles, thus affecting their practical applications. Hence, it is very important to investigate how the concentration of dopant doped semiconductor nanoparticles affects electrical properties and optical from the viewpoints of principle physics and applications, in which work on optical and high-temperature electrical properties of pure and Ni doped CuO nano crystals. The nanocrystals of CuO and Ni doped CuO were achieved through wet chemical precipitation route and the elemental composition of the as prepared was verified by EDX analysis (Firdous et al. 2013).

In this thesis, photoactive materials containing Ni doped Cu_2O with high quality and stability were prepared by using economical, simple and reliable electrodeposition method based on underpotential deposition (UPD). Linear sweep voltammetry (LSV) technique was used to dope nickel. Prepared materials were characterized using EDX,

SEM, XRD, UV-Vis spectroscopy and electrochemical techniques. The photoelectrocatalytic performances of Ni doped Cu_2O photoelectrodes depending on the amounts of nickel doping were determined and the change in photoelectrocatalytic activities was studied comparatively.

2. LITERATURE REVIEW

Martinez-Ruiz et al. studied the electronic properties of bulk Cu_2O, clean and doped with Ag, Ni and Zn. By using first principles total energy calculations. In which clean Cu_2O was cubic as calculated ground state structure that was lattice constant a = 4.30 Å, and bulk modulus B_0 = 108 GPa are in excellent agreement with experimental values a = 4.27 Å, and B_0 = 112 GPa. Cu_2O is a semiconductor material with a small direct band gap at the point, in its ground state. Calculated experimental value of ∼2.0 eV is larger than the value of ∼0.5 eV, reflecting the problems of local density functional theory calculating the excited states. It is results in a reduction of the band gap, doping with Ag. This result is significant, because it implies that the band gap of Cu_2O could be engineered by variable the ratio of Ag in the crystal. P-type semiconductor raised in doping with Ni with the impurity levels above the valence maximum, while doping with Zn results in a n-type semiconductor, with impurity levels above the conduction band minimum (Martinez-Ruiz et al. 2003).

Kikuchi and Tonooka were studied on properties of electrical and structural of Ni doped Cu_2O (Cu_2O: Ni) films, in which prepared by the pulsed laser deposition (PLD) from CuO:Ni. With increasing Ni content the mass fraction of Cu_2O in the films decreased, while assigned the remaining fraction to CuO semiconductor by X-ray diffraction measurements. By increase in the deposition temperature of both Ni doped and undoped films lead Cu_2O fraction of the films became 100%, reduction process from CuO to Cu_2O was depressed by Ni doping and hall measurement indicated the properties of carrier transport Cu_2O:Ni films was a p-type semiconductor. The carriers generated by Cu-vacancies in Cu_2O. It detected that the doped Ni atoms enter the in Ni doped Cu_2O semiconductor film and produce the scattering center of the neutral impurity, resulting in low mobility.

Kikuchi et al. were study on Ni doped and undoped cuprous oxide (Cu_2O) films, with the mobility and density of hole carriers, in which prepared by pulsed laser deposition from Ni doped and undoped CuO goals, respectively, which measured to examine the mechanisms of transport and carrier generation in doped films. The carrier density of the films revealed in temperature dependence of the present of Ni, indicate the activation energies level of acceptor from the films were 0.22–0.25 eV. The mobility of the films was changed from 0.58 to 0.0 in temperature dependence when doping with Ni. Result was an evidenced which hole carriers in Ni doped Cu_2O whereas in undoped Cu_2O obtained by Cu vacancies and mainly scattered by neutral impurity scattering centers. Measurements of the films by X-ray diffraction (XRD) revealed increasing Ni content cause the decreased mass fraction of Cu_2O in the films, while increased CuO. Then detected the reduction process of CuO to Cu_2O was suppressed by the Ni doping (Kikuchi et al. 2006).

Sieberer et al. were investigate the influence of transition metal substitution in Cu_2O on the basis of *ab initio* calculations employing density-functional theory GGA+U, used the super cell approach. In which work effect of substituting Cu by Mn, Fe, Co, and Ni, assuming both low transition metal concentrations 3.2% in a cubic geometry and higher transition metal concentrations 9.1% in a trigonal setup. To elements Co and Mn constants of magnetic exchange up to the fifth nearest adjacent are calculated, assuming both cases, perfect Mn/Co:Cu_2O as well as defects in the host such as single copper and oxygen vacancies. Results openly illustration the importance of defects in these materials and thus offer an explanation for different, seemingly reverse, experimental results (Sieberer et al. 2007).

Ahmed and Gajbhiye were study to port the synthesis and characterization of Cu_2O semiconductor nano rods doped with Mn, Ni and Co transition metal ions and the study of their magnetic properties. It was used modified polyol method. In which powder X-ray diffraction patterns clearly indicated them to be poly crystalline single phase material. Results ferromagnetic behavior was found to be dependent on the doped concentration and increased consistently with its increment in the material. The presence of the defects was supported by the room temperature photo luminescence reading which showed that intensity of the peaks was dependent on the dopant. There was strong correlation among

the magnitude of the photo luminescence peak and the detected ferromagnetic property in the doped samples (Ahmed and Gajbhiye 2010).

Ma et al. studied to grown cuprous oxide (Cu_2O) films by electrodeposition in aqueous solutions of different pH and investigated the influence of bath pH on structural, morphology, and photoelectrochemical (PEC) properties of Cu_2O films. XRD indicated that all prepared films were polycrystalline Cu_2O, without creation of competing phases like CuO and Cu. The Cu_2O crystallites formed in the solution with a pH of 8 by film grown with preferential (200) planes exposed and the films deposited in solution at pH = (10, 12 and 14) reveal Cu_2O crystallites with preferential (111) planes exposed. The Cu_2O film grown in the solution at pH = 12 appearances the best PEC performance for hydrogen generation. The (111) facets of the Cu_2O film were stable without corrosion during the PEC test. A mechanism for the preferred faceting in alkaline solution has been discussed (Ma et al. 2015).

Wick and Tilley studied to **c**uprous oxide is a promising material with the ability for low cost, large-scale solar energy conversion attributed to the abundant nature of copper and oxygen, proper band gap for absorption of visible light, which effective, few energy intensity fabrication processes like electrode position. To the photoelectrochemical (PEC) water splitting, protective over layers have been advanced that importantly extend the durability of hydrogen-evolving Cu_2O-based semiconductor materials. New developments from the advancement of protective over layers for stabilizing photo absorber materials for water splitting are discussed, and it is concluded that the utilize of protective over layers is a viable strategy for practical water splitting instruments (Wick and Tilley 2015).

Shyamal et al. worked to improvement of p-Cu_2O semiconductor thin films by cathodic electrode position technique at constant current of 0.1 mA/cm^2 on Cu, Al, and indium tin oxide (ITO) substrates in basic $CuSO_4$ solution containing Triton X-100 as the surfactant at 30−35 °C. In which semiconductors characterizations carry out by used UV−vis spectroscopy, scanning electron microscopy (SEM), X-ray diffraction (XRD), and Raman spectroscopy. Band gap energy of semiconductor determined as ∼2.1 eV, while SEM illustrated that the surface morphology is covered with Cu_2O semiconductors. The water

reduction ($H_2O \rightarrow H_2$) in pH 4.9 aqueous solutions from photoelectrochemical over the different substrates differ in the order of Cu > Al > ITO. The highest current of 4.6 mA/cm2 has been saved over the Cu substrate however at a low lighting of 35 mW/cm^2, which is significantly greater than the values (2.4 mA/cm^2 on Au coated FTO or 4.07 mA/cm^2 on Cu foil substrate at a lighting of 100 mW/cm^2) reported in literature (Shyamal et al. 2015).

Liang et al. studied to fabricate a Cu_2O/NiO_x composite photocathode by spin coating a thin film of NiO_x on Cu_2O photocathode to improve its stability and photocurrent. Results illustrated that NiO_x layer on Cu_2O had a trade-off influence on photocathode performance. The thicker of NiO_x film on Cu_2O, the lower of the photocurrent, but high stable of the Cu_2O electrode. In optimal 240 nm thickness of NiO_x layer, the Cu_2O/NiO_x composite photocathode extracted excited electrons effectively, and a H_2 production rate of 5.09 $\mu Lh^{-1}cm^{-2}$ was obtained from a MPEC under continuous light illumination with 0.2 V external bias. By tuning the synergistic effect of bioanode and photocathode, MPEC could provide a feasible solution on simultaneously organic conversion and energy restoration from wastewater and solar light (Liang et al. 2016).

Yang et al. worked to prepared Cu_2O/CuO bilayered composite by a facile method that involved an electrodeposition and a subsequent thermal oxidation. Obtained results Cu_2O/CuO bilayered composites revealed a surprisingly high activity and more stability toward PEC HER, expecially at high potentials in alkaline solution. In which the density photocurrent of HER was 3.15 $mAcm^{-2}$ at the potential of 0.40 V *vs*. RHE, which was one of the two highest reported at the same potential on copper-oxide-based photocathode. This study reveals the potential of the Cu_2O/CuO bilayered composite as an improving photocathodic material for solar water splitting (Yang et al. 2016).

Shooshtari et al. worked on surface engineering of bulk Cu_2O photocathode thorough employing nano structured materials. To synthesized nanorods of copper oxide with average lengths of 150 nm by anodization of Cu foil in aqueous electrolyte, followed by annealing treatment. Some heating processes were examined to get pure Cu_2O nanostructures and lastly the moderate. Annealing procedure at 700 °C under gas flow resulted as pure Cu_2O nanostructures, confirmed by XRD analysis. Surface modified

nanorod/bulk Cu_2O electrode was ready by spin coating of sediments suspension of anodized drop on bulk Cu_2O film fabricated by thermal oxidation method, followed by final heating process. This novel bulk Cu_2O electrode with modified nanostructured surface can be a good candidate as the electrode of either photoelectrochemical systems for hydrogen obtained or the photocathode of bulk hetero junction photo voltaic cells (Shooshtari et al. 2016).

Yang et al. worked to improve photo electrochemical (PEC) stability of cuprous oxide (Cu_2O), by using the p-type Cu_2O films containing metallic copper inclusions, which are electrodeposited by controlling the concentration of sodium dodecyl sulfate in the plating solutions. In which concentration of sodium dodecyl sulfate increase to 1.70 mM. The deposited Cu_2O films change from n-type to p-type semiconductor, until the PEC stabilities of p-type Cu_2O films reach 99.23% without bias and 86.34% with bias, which are significantly greater than the n-type Cu_2O films or the pure p-type Cu_2O without copper inclusions. The crystal morphology, structure, and composition of the Cu_2O films are characterized, and the effect of Cu inclusions on the PEC stability is interpreted through the energy band diagrams (Yang et al. 2016).

Maijenburg et al. studied the absence or presence of a protective layer of RuO_2 material. From principle of instability of p-Cu_2O semiconductor thin films deposited on a platinized Si substrate when used as photocathode in photo electrochemical water splitting, applied at +0.3 V vs. RHE and at pH 7, p-Cu_2O films were found to indicated a slightly most stable performance as compared to photo electrochemical measurements reported in the literature at 0 V vs, RHE and under acidic conditions. In addition, when H_2O_2 was added to the electrolyte the stability and the photocurrent induced by the Cu_2O semiconductor films significantly improved, which is clarified by yielding oxygen, efficient scavenging of electrons, and water as performed by gas chromatography (GC). Results provided in this work rationalize the attachment of an impact H_2 evolution catalyst as a means to significantly improve the stability of p-Cu_2O semiconductor electrodes (Maijenburg et al. 2017).

Zhang et al. worked the Si/Cu_2O heterojunction nanowire arrays were fabricated by the in-situ thermal decomposition of $Cu(NO_3)_2$ on silicon nanowires. Which different

methods has been developed to fabricate like heterojunctions, as the potential applications of nanostructured Si/Cu_2O heterojunction in electronic and photoelectronic devices, the nanoparticles Cu_2O decomposed illustrated that uniformly distributed on the surfaces of Si nanowires. In which chemical composition, microstructure states of the products were investigated. Used as photoanodes for photo electrochemical water splitting, the Si/Cu_2O heterojunction nanowire arrays exhibited a maximum photocurrent density of 4 mA/cm^2 at 1.23 V vs. RHE and an onset potential of 0.62 V vs. RHE (Zhang et al. 2017).

Xue et al. studied to prepared smooth and uniform Cu_2O thin films and investigated the influence of Au nuclei layer on the production of these thin films by scanning electron microscopy (SEM), X-ray photoelectron spectroscopy (XPS), atomic force microscopy (AFM), and the optical absorption (UV–vis/DR) methods. When the electrodeposition is conducted after sputtering Au nuclei layer on ITO, smooth and uniform Cu_2O thin films without any islands and pinholes are produced. Au nuclei layer provides more surface area, improves the Cu^{2+} ion migration, and subsequently raised the deposition of Cu_2O nuclei on Au nuclei layer to produce smooth and uniform Cu_2O thin films. More ever the Au nuclei layer plays major role in improving photo electrochemical performance of Cu_2O thin films (Xue et al. 2017).

Du et al. studied to prepared CuO/Cu_2O semiconductor photocathodes on fluoride doped tin oxide (FTO) substrate by simply annealing the electrodeposited Cu_2O, in which characterized by X-ray diffraction (XRD), transmission electron microscope (TEM), scanning electron microscopy (SEM), UV–vis absorption spectra and X-ray photoelectron spectroscopy (XPS). Result indicated the heterojunction of CuO/Cu_2O semiconductor was formed in the presented the nature of p-type semiconductor during the annealing process. The photoelectrochemical (PEC) stability and photocurrent density of the p-type heterostructure CuO/Cu_2O semiconductor photocathode was improved greatly compared with the pure Cu_2O semiconductor, which was significantly affected by temperature and annealing time. The highest stability was obtained via annealing at 650 °C for 15 min (at −0.3 V vs. Ag/AgCl) and highest photo current density of −0.451 mA/cm2, which gave a remarkable improvement than the as-deposited Cu_2O semiconductor (−0.08 mA/cm^2). This suggested that the CuO/Cu_2O semiconductor

heterojunction make easy the electron-hole pair separation and enhanced the stability and photocathode's current (Du et al. 2017).

3. MATERIALS AND METHODS

3.1. Materials

3.1.1. Chemicals

Copper sulphate pentahydrate ($CuSO_4.5H_2O$), nickel sulphate ($NiSO_4$), sodium sulphate (Na_2SO_4), lactic acid ($C_3H_6O_3$), sodium hydroxide (NaOH), sulfuric acid (H_2SO_4), ethanol (C_2H_6O), acetone (C_3H_6O).

3.1.2. Instruments

Precision balance: Denver Instrument SI-234
PH meter: Orian 3 Star
Ultrasonic mixer: Apple S 60 H
Deionized water device: Human Power 1
Electrochemical analyzer: CHI 6096 E
X-ray diffractometer (XRD): Rigaku Ultima IV
Scanning electron microscope (SEM): JEOL JSM-6510
Energy dispersive dpectrometer (EDX): JEOL JSM-6510
UV-VIS-NIR spectrophotometer: Shimadzu UV-3600
Solar simulator: Solar Light 16S-002

3.1.3. Electrochemical Studies

Electrochemical processes that make up a significant part of the work; analyzed substance, solvent, electrolyte and an electrode from an electrochemical cell and an electrochemical device known as potentiostat/galvanostat. We need to pay attention to the

selection of materials to be used for electrochemical studies. The particulars are mentioned below.

3.1.3.a. Properties of Solvent

Starting with electrochemical studies, first it is necessary to investigate the chemical and physical properties of the solvent in detail. The solvents are used at a high degree of solubility, high electrical conductivity and very high purity. It should have dielectric constant, and should not enter into reaction. Furthermore, if pure water is used as the solvent, must be distilled water or higher purity production ultrapure water systems use. We used GFL 2008 brand deionization system in our studies.

3.1.3.b. Solutions

In our studies, we found that aqueous basic solutions containing 0.02 M $CuSO_4$, 0.2 M Na_2SO_4 and 0.3 M lactic acid solution, such as an environment that prepared by Cu_2O semiconductor materials were used by electrochemical method. The pH of the solutions was 8.5 that prepared by adjusting with pH meter using NaOH and H_2SO_4. For nickel doping, nickel solutions in different concentrations (0.0001, 0.0002, 0.0004, 0.0008, 0.001, 0.002, 0.004 and, 0.008 M) were used. For photoelectrocatalytic measurements, 0.1 M Na_2SO_4 solution was used.

3.1.3.c. Electrochemical Cell

Electrochemical reactions can be performed in cells with two or three electrodes. Both of the cathode electrodes and anode electrodes are immersed in an electrolyte solution. Thus, the oxidation/reduction (redox) reactions take place, it’s clear that the reduction reactions take place in the cathode electrode, and also the oxidation reactions take place in the anode electrode. In addition, usually the electroactive in cells consisting of three electrodes dissolving the compound and the electrolyte dissolved in the solution, the counter and reference electrode (Goodridge and King 1974). Another important factor is the use of unfractionated cells where the three electrodes are placed in separate

compartments in electrochemical processes and the opposite, the study, in which the reference electrode is placed in one compartment as shown in Figure 3.1.

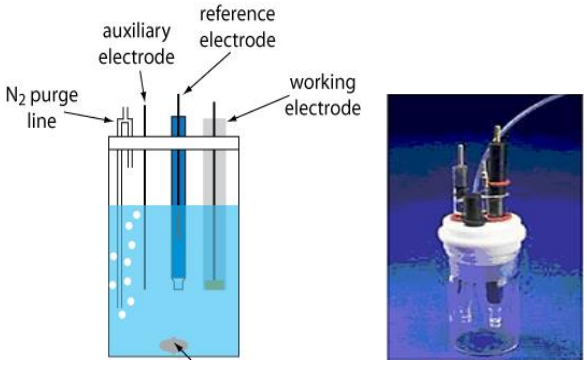

Figure 3.1. Electrochemical cell

3.1.3.d. Electrodes

In our studies, we used three kinds of electrodes: reference, counter and working electrodes reference electrode, is one of the electrodes that have a half-cell knowing and fixed potential, with properties that is independent of its composition of electrolyte desired. These electrodes are used for potentially controlled electrolysis and voltammetry techniques; therefore, the reference electrode should be used so as to determine the potentials (Skoog et al. 1998). As well the reference electrode must be easily prepared, stable, with a specified current range. It must be having reversely and should not change over time. Generally, reference electrodes are silver silver chloride (Ag/AgCl) and saturated calomel reference electrode (SCE) used (Erdoğan 2009).

In our studies, Ag/AgCl and SCE reference electrodes used in the electrochemical preparation of Ni doped Cu_2O photoelectrodes and photoelectrochemical studies, respectively. Some good properties of Calomel electrode: it's very easy prepared because of the ease of preparation of analytical chemists an electrolyte mercury-mercury chloride reference electrode; mercury and calomel in (Hg_2Cl_2), potassium chloride (KCl) solution formed into a platinum wire for external connection. An immersed half-cell is used as shown in (Figure 3.2). The potential of this half-cell depends on temperature and potassium chloride concentration of the reference electrode.

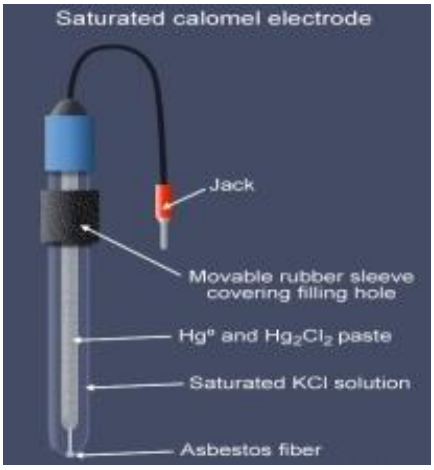

Figure 3.2. Saturated calomel electrode

The potential of saturated calomel electrode is 0.224 V due to faulty potential connection in case of potential connection to standard hydrogen electrode, liquid connection. However, when there is no fluid connection, this value is around 0.241 V (URL-1 2015). Figure 3.3 shows the potential change as a function of temperature. The potential values of the calomel electrode versus the standard hydrogen electrode (SHE) at 0-100 °C,

$$E_T = 0{,}244 - 0.00072\ (T - 25) \qquad (3.1)$$

According this Equation (3.1) the potential change as a function of temperature as shown in Figure 3.3 at (12-50 K), on the other hand, the potential of the reference electrodes can change over the time, it should be preserved in a solution.

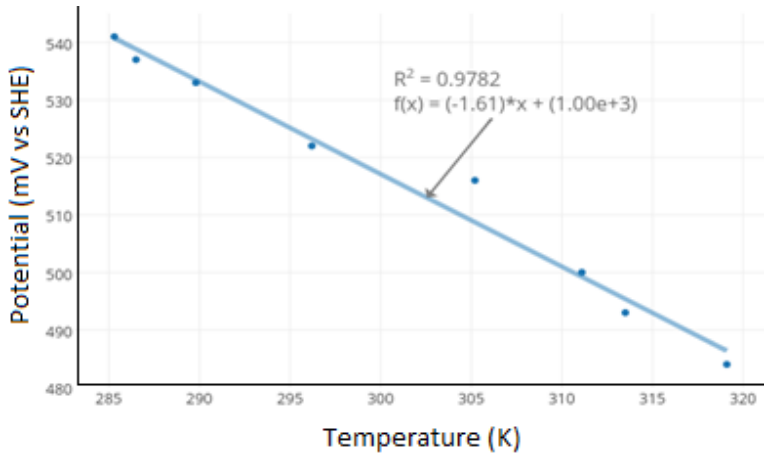

Figure 3.3. Change of electrode potential with temperature

The Ag/AgCl reference electrode was obtained by immersing Ag in an agitated solution after agglomeration with AgCl in the electrolytic solution (Figure 3.4).

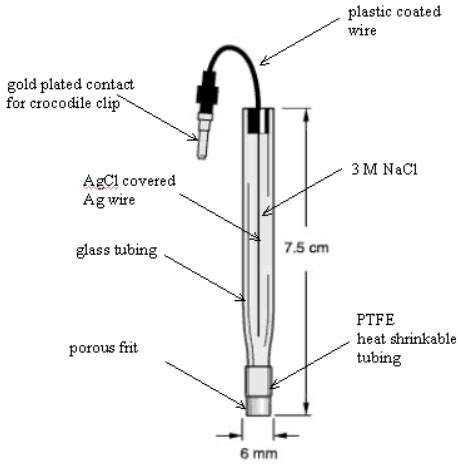

Figure 3.4. Ag/AgCl reference electrode

The potential of Ag/AgCl electrode is 0,222 V against standard electrode potential SHE. This value for SCE is 0.268 V. On the other hand, the concentration of KCl affects the electrode potential for both Ag/AgCl and SCE. For example, when the molar concentration of KCl for the calomel electrode is taken as 1.0 and 0.1 M, the voltages at 25 ° C are 0.282 and 0.334 V, respectively. Generally, Ag/AgCl electrodes can be used when working above 60 °C with calomel electrodes.

The working electrode is the most important part of the electrolysis system. By the way, the counter electrode has no effect on the reaction occurring in the working electrode. And also the counter electrode is used to complement the circuit and feeds the working electrode with electrons. For the more, a small current is observed in the counter electrode due to the non-process electrolyte types in the working electrode. Therefore, the counter electrode process is not interested. Several uses of platinum wire as counter electrode are because of its nature inert in electrochemical studies as shown in (Figure 3.5).

The working electrode is the electrode at which the analyte is oxidized or reduced. The potential between the working electrode and the reference electrode is controlled. Electrolysis current passes between the working electrode and a counter electrode. The

working electrode acts as an anode material in which an oxidation reaction takes place during oxidation in an electrochemical cell, and also cathode material during which the reduction reaction takes place during reduction. Moreover, the preference of the cathodic and anodic working electrode is important (Weinberg 1972). For this reason, surface morphology and activity must be taken into account in the preference of the electrode material. In our studies, ITO (indium tin oxide) coated glass was used as the working electrode, platinum wire was used as the counter electrode, and Ag/AgCI and SCE were used as the reference electrode.

Figure 3.5. Platinum counter electrodes

3.1.3.e. Potentiostat

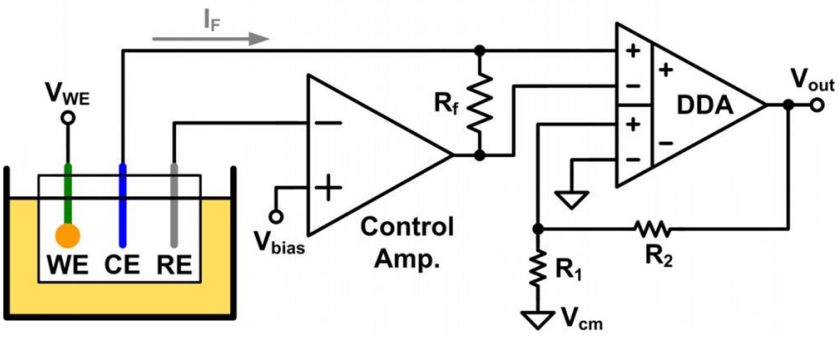

Figure 3.6. Schematic representation of potentiostatic components used in electrochemical studies

Potentiostat is an electronic device that regulates the potential of the working electrode versus the reference electrode. This is used in potentially controlled electrolysis. The linearly scanned potential generator, similar to the integration circuits, is the signal source as shown in Figure 3.6.

The output signal from the source first comes to the potential control circuit. And also the electrical resistance is very large (> 10^{11} Ω) for a small amount of current flow in the control circuit containing the reference electrode, this ensures that all of the current from the source is transferred from the opposing electrode to the working electrode. In addition, in the potentiostat process, the current measuring circuit is connected to the working electrode. Moreover, the potential tracer connected to the reference electrode constantly indicates the potential of the electrode which it is connected. Although, the control circuit adjusts this current to ensure that the potential between the reference electrode and the working electrode is equal to the output potential of the linear voltage generator, the measured potential is the potential between the work and the reference electrode. Finally, during the test run the working electrode is at the known true potential and this potential is recorded as a function of time (Erdoğan 2009).

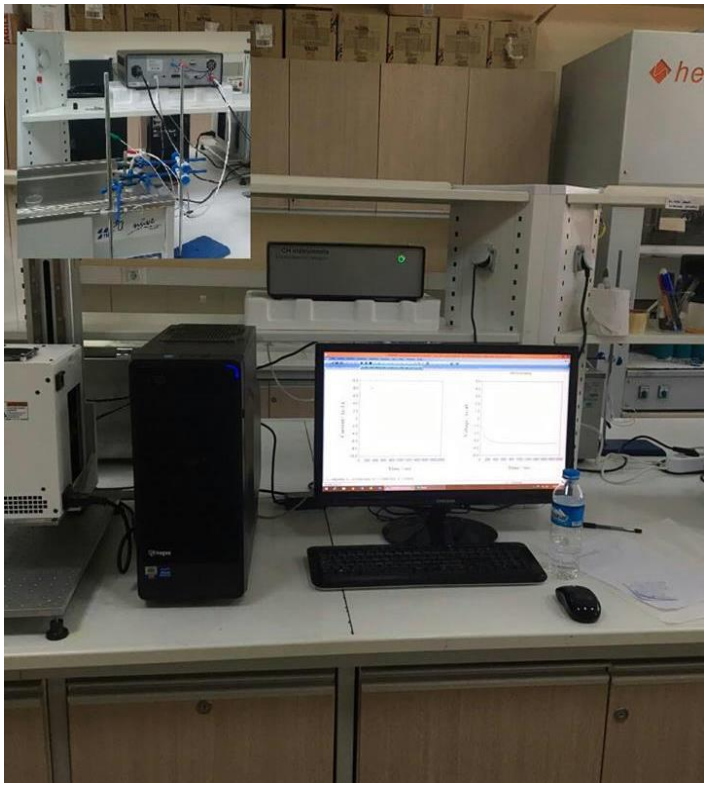

Figure 3.7. A photo of the potentiostat system used in our studies

Photoelectrochemical studies were carried out with a CHI electrochemical analyzer (CHI 6096 E Inc., USA) in a three-electrode configuration with, indium tin oxide (ITO) coated

glass as working electrode, Platinum wire (Pt) as a counter electrode, Ag/AgCl and standard calomel electrode SCE as the reference electrode. In our studies we used (CHI 6096E USA) type operational potentiostat in our studies (Figure 3.7). It alternating voltammetry through potentiostat, potentially controlled electrolysis and amperimetric techniques were used for analysis.

3.2. Methods

3.2.1. Electrochemical Methods

Voltammetry, an electroanalytical method used in electrochemistry, on the condition that a working electrode is polarized so that information about the analyte can be obtained, (Skoog et al. 1998), in which the flow is measured in the form of a potential function to be applied. To provide the voltammeter polarization, the surface area of the working electrodes is taken to be a few millimeters square, and a few micrometers square (Heyrovsky 1922). Using mercury electrode as a microelectrode is the most important difference that separates polarography, a special type of voltammetry, from other voltammetric techniques. Voltammetry used for many analytical purposes, is widely used for non-analytical purposes. As an example, in the investigation of adsorption processes on the surface, examination of the oxidation / reduction processes occurring in various media, as elucidation of electron transfer mechanisms occurring on chemically modified electrode surfaces (Erdoğan 2009).

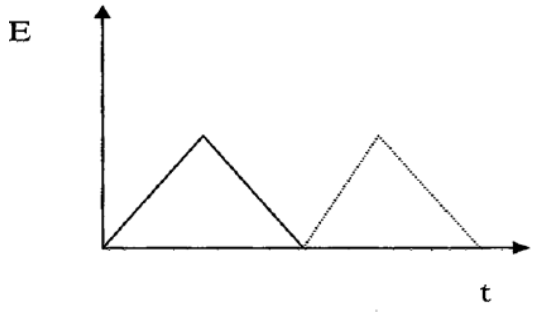

Figure 3.8. Cyclic voltammetric technique for conversion the potential vs time

The cyclic voltammetry is increased in potential linearly as a function of time up to a certain potential value and returned to its starting potential again as shown in (Figure 3.8).

The graphs of the potential versus current values obtained by using the alternating voltammetry technique are called voltamograms. Usually, electrochemical information is given in the form of these graphs (Malachesky 1969). Potential values and currents can be measured at the same time when the reaction occurs in an electrochemical cell. The potential of the working electrode is changed between the values determined in the negative and positive direction based on the potential of the reference electrode by means of a potentiostat. Electrode potential is scanned in the positive direction and a current is generated by the presence of molecules or ions in the environment reaching the oxidation potential. This flow is called the anodic current. If the electrode is to be scanned on a potentially negative side, a current will be generated due to the reduction of the electroactive substances when the ions or molecules in the environment reach the reduction potential, and the generated current is called the cathodic current (Skoog et al. 1998).

For a cyclic electrode response, there must be a voltage difference between the cathodic peak potential (Epc) and the anodic peak potential (Epa) (0.059/n) V. The formal potential (E^o) of the redox couple examined is equal to the midpoint of these two peak potentials. For an alternating voltamogram, the ratio of anodic peak current to cathodic peak current is approximately one ($I_{pa} / I_{pc} \cong 1$).

$$Ox + ne^- \leftrightarrow Red \qquad (3.2)$$

For Equation 3.2, the amount of oxidant on the surface decreases with time, so the current will fall and the reaction will end. Thus, a selective reaction will be realized by adjusting potential. The reference electrode is used in addition to the working electrode and the counter electrode. According to the Nernst equation, as the concentrations of the electroactive substances change with time, the potential of the working electrode is always kept constant by using the potentiostat.

According to the Nernst equation (Equation 3.3) for Equation 3.2, the concentration of oxidant will decrease over time and will potentially change with time. The oxidant in the environment, it will remain at fixed value for the potential short-term with the exhaustion of the whole (Erdoğan 2009).

$$E = E^{\circ} - \frac{RT}{nF} \ln \frac{[Red]}{[Ox]} \tag{3.3}$$

E_{cell} is the cell potential,

E°cell is the standard cell potential,

R is the universal gas constant: R = 8.314472(15) J K^{-1} mol^{-1},

n is the number of moles of electrons transferred in the cell reaction or half-reaction,

F is Faraday constant, the number of coulombs per mole of electrons,

F = 9.64853399(24)×10^4 C mol^{-1},

T is the temperature in kelvins at room temperature (25 °C),

RT/F may be treated like a constant and replaced by 25.693 mV for cells.

3.2.2. UV-VIS Spectroscopy

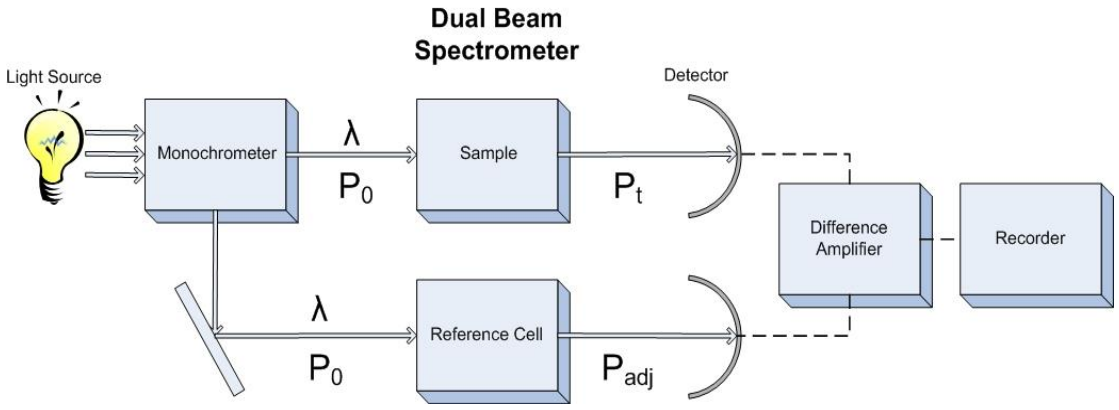

Figure 3.9. Schematically representation of double beam spectrometer

Molecular absorption spectroscopy is the method of measuring the absorbance (A) or permeability (T) of a solution in a cell by using the wavelengths. Absorption in the ultraviolet and visible region is mainly due to the stimulation of the bonding electrons in

the molecules. As a result, the wave lengths of the absorption peaks with the types of bonds in the species studied and are thus used in the quantitative determination of functional groups in a molecule as well as of compounds carrying functional groups (URL-2 2015). The components of the double-light-path spectrometry are shown in Figure 3.9.

The components of the double-light-path spectrometry are shown in Figure 3.9. In the first the light comes from the light source to a monochromator. And then the light from the monochromator is sent to the reference and sample cells, separated by two equal wavelengths. These two light beams sent to the sample cell and reference cell are detected with two different detectors. Finally, the permeability value of the reference cell and the permeability value of the sample cell are continuously compared in the signal readout, and the ratio of the generated signals is read. The spectrophotometer used in our studies is shown in Figure 3.10.

Figure 3.10. Shimadzu UV-3600 UV-VIS-NIR spectrophotometer used in our studies

3.2.3. SEM

Scanning Electron Microscopy (SEM) is a powerful method for the investigation of surface structures of Molecules, this technique provides a large depth of field, which means, and the area of the sample that can be viewed in focus at the same time is actually

quite large. SEM has also the advantage that the range of magnification is relatively wide allowing the investigator to easily focus in on an area of interest on a sample that was initially scanned at a lower magnification. Furthermore, the three-dimensional appearing images may be more appealing to the human eye than the two-dimensional images obtained with a transmission electron microscope. Therefore, an investigator may find it easier to interpret SEM images. Finally, the number of steps involved for preparing specimens for SEM investigation is lower and thus the entire process is less time consuming than the preparation of samples for investigation with a transmission electron microscope.

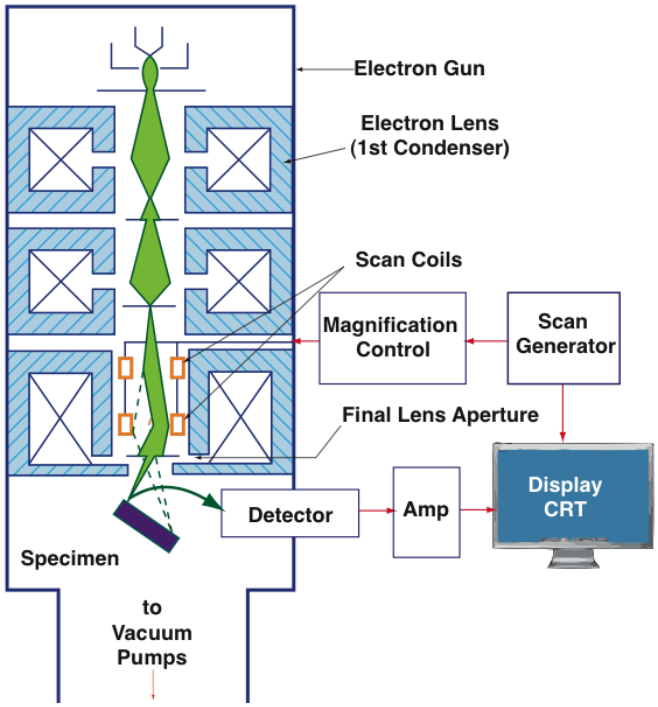

Figure 3.11. Schematically representation the main components of SEM column scanning system

Essential components of all SEMs include electron column, scanning system, detector, display, vacuum system and electronics controls. Infrastructure requirements: rower supply, vacuum system, cooling system beam condenser, vibration-free floor, room free of ambient magnetic and electric fields. SEMs always have at least one detector (usually a secondary electron detector), and also most have additional detectors as shown in (Figure 3.11). The electron column of the SEM consists of an electron gun and two or more electromagnetic lenses operating in vacuum. The electron gun generates free

electrons and accelerates these electrons to energies in the range 1-40 Kev in the SEM. The purpose of the electron lenses is to create a small focused electron probe on the sample. Most SEMs can generate an electron beam at the specimen surface with spot size less than 10 nm in diameter while still carrying sufficient current to form acceptable image. Typically, the electron beam is defined by probe diameter in the range of 1 nm to 1 μm. In order to produce images, the electron beam is focused into a fine probe, which is scanned across the surface of the sample with the help of scanning coils. Moreover, each point on the specimen that is struck by the accelerated electrons emits signal in the form of electromagnetic radiation. Selected portions of this radiation, usually secondary or backscattered electrons are collected by a detector and the resulting signal is amplified and displayed on a computer screen or computer monitor.

The SEM has a large depth of field about 30 mm, which allows a large amount of the sample to be in focus at the same time and produce an image that is a good representation of the three-dimensional sample. In addition, the combination of higher magnification, large depth of field, greater resolution, commotional and crystallographic information makes the SEM one of the most highly used in lab searches area and industry. A SEM may be equipped with an EDX analysis system to enable it to perform compositional analysis on specimens. EDX analysis is useful in identifying materials and contaminants, as well as estimating their relative concentrations on the surface of the specimen (Stadtlander 2007).

3.2.4. EDX

Energy-dispersive X-ray spectroscopy (EDX) is a type of spectroscopy used by SEM to provide information on the chemical composition of the sample being examined in the SEM (Figure 3.12). Compared to other spectroscopic techniques used for the same purpose, it is quite advantageous. In EDX, when the electron beam transmitted to the sample interacts with the atoms of the sample, the energy is around 10-20 keV, causing X-ray photons to spread through the sample. Detection of these emitted photons is carried out by means of an energy separation spectrometer. EDX is based on the principle that the produced x-rays are measured as a function of the energy, and the chemical composition of the sample to be examined is determined according to the properties of

the X-rays emitted from the sample. The portion of the sample to be analyzed may be the entire sample, a region, or any point. Thus, chemical analysis of any desired region during image acquisition can be performed. The energy of x-ray photons generated by sending an electron beam depends on the characteristics of the sample under investigation. As the emitted electrons form x-rays in the inner regions rather than the sample surface, EDX does not give information about the surface properties. In addition, Also, it is not very useful to use it in EDX analyzes because the X-ray intensity of elements with low atomic number is low. The fact that the EDX analysis can be performed at the same time as the acquisition of the SEM image, and the analysis without making the sample dissolve by any means, is a significant advantage of EDX (URL-3-4 2016). The EDX system used in our studies (JEOL JSM-6510) shown in Figure 3.12.

Figure 3.12. The EDX and SEM system we use in our studies (JEOL JSM-6510)

3.2.5. XRD

The X-ray diffraction method is widely used in the determination of crystal structures. XRD devices have improved significantly after the Fourier Transform revolution. Sharp wide angle, short time and suitable output devices were analyzing each angle individually prior to offering a collective value. The ability to collect fingerprint sensitive data in crystal structures makes XRD very useful and reliable. The XRD Crystal is a technique

that can determine the distance between atomic planes. The working principle is based on the collection of scatter and diffraction data by sending and scanning the x-ray to the sample to be analyzed. The X-rays are sent to a crystal plane and reflected by the crystal plane of the atoms, which is an X-ray diffraction phenomenon. This actual reflection is different from the reflection of the light from a mirror plane. Diffraction is not a superficial phenomenon. In other words, incoming x-rays reach the plane of the atoms beneath the crystal surface.

Wavelength fixed X-rays are used in XRD studies. To obtain these x-rays, electrons emitted by heating a filament, such as tungsten, is accelerated in the field and accelerated to an electron beam which is energized with high energy. These electrons reach the anodic electron shells (Skoog et al. 1998). If the electron beam collides with an electron in the shell near the core, the electron is removed from its position and the atom becomes unstable due to electron loss. When If the vacant electron fills an electron in the higher energy crust shell, an energy difference occurs due to this electron transition, and this energy difference is spread as a photon of X-rays. The XRD device used in our studies is shown in Figure 3.13.

Figure 3.13. The XRD device (Rigaku Ultima IV)

A way in which the rays reflected by the atomic planes collide with the X-ray beam at a certain angle, known as the Bragg angle, which is equal to the exact multiple of the wavelength (λ), the rays will have the same phase and the diffraction will occur come to a point. It is shown in Figure 3.14, to obtain the diffraction peak; It is necessary to have a relation between the angle of attack (θ) of the x-rays to the atomic planes, the distance (d) between the atomic planes and the wavelength λ of the incoming X-rays, the difference between the lengths of the paths that X-rays take it (Erdoğan 2009).

X-ray diffraction is a powerful tool to study the crystal structure of semiconductors. XRD gives information about crystalline phase, quality, orientation, composition, lattice parameters, defects, stress, and strain of samples. Every crystalline solid has its unique characteristic X-ray diffraction pattern, which is identified by this unique ‘‘fingerprint’’. Crystals are regular arrays of atoms and they are arranged in a way that a series of parallel planes separated from one another by a distance d. Figure 3.14 shows the detail of the process of x-ray diffraction. If an x-ray beam with a wavelength strikes the sample with an incident angle, then the scattered ray is determined by Bragg’s law (n = 2dsin). Where n is an integer, is the wavelength of the beam, d is the spacing between diffracting planes, and is the incident angle of the beam. The set of d-spacing in a typical x-ray scan provides a unique characteristic of the samples in question (Amin and Willander 2012).

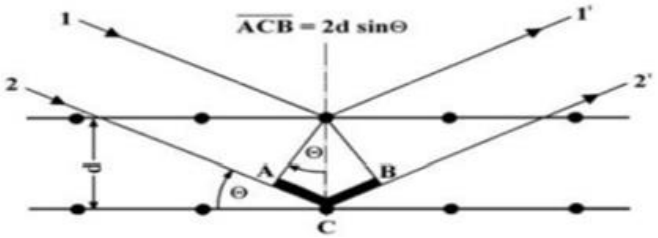

Figure 3.14. Schematic diagram of Bragg's reflection from lattice planes in a crystalline structure with by development of X-ray diffraction

$$ACB = AC + CB \tag{3.4}$$

$$\sin\theta = AC / d = CB / d \tag{3.5}$$

$$AC = CB = d \sin\theta \tag{3.6}$$

The difference between the lengths of the paths of the X-rays is given by Equation 3.7 below.

$$AC + CB = 2d \sin\theta \quad (3.7)$$

$$ACB = 2d \sin\theta \quad (3.8)$$

In order for the diffraction to be possible, this path difference must be equal to the multiple of λ or λ. Thus Equation 3.8 can be written (Erdoğan 2009).

$$ACB = n\lambda \quad (3.9)$$

$$2d \sin\theta = n\lambda \quad (3.10)$$

3.2.6. Photoelectrochemical System

The photoelectrocatalytic performances of these oxides formed on ITO coated glass electrodes were measured under sunlight, which is represented by a three-electrode system (Figure 3.15). The photoelectrochemical measurements were recorded under a beam of AM 1.5G using a Solar Light-16S-002 brand solar simulator with a 150 W xenon arc lamp. The photocurrent-potential, and photocurrent-time curves were measured using linear sweep voltammetry and chronoamperometry techniques, respectively.

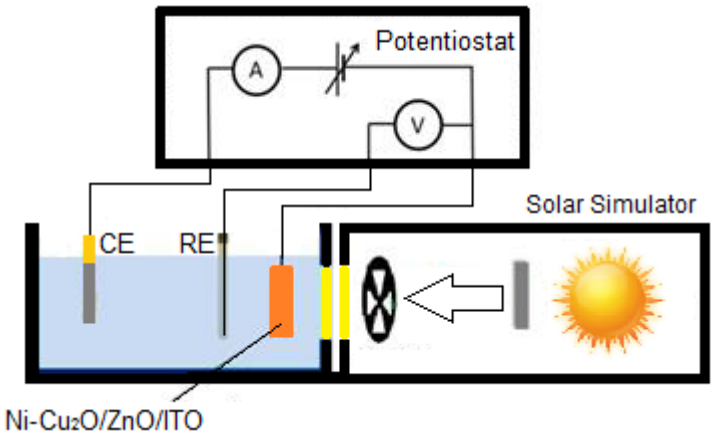

Figure 3.15. Schematic representation of the instrument used for photoelectrochemical measurements

4. RESULTS AND DISCUSSION

4.1. Electrochemical Studies

In this thesis study, the synthesis of homogeneous Ni doped Cu_2O materials with various compositions using electrochemical technique was reported. The general experimental strategy employed in this thesis study was the atom-by-atom growth of Cu_2O materials using the UPD of copper element. In principle, UPD, the electrochemical deposition of a metal onto a substrate at potentials more positive than the Nernst potential, is usually restricted to the formation of one atomic layer of the deposited metal. The UPD potential for Cu were determined by cyclic voltammetric measurements. In order to determine a deposition potential of the Cu_2O from the solution, the cyclic voltammetric measurements of copper were also recorded at the UPD region in the aqueous medium. The results showed that the bulk copper deposition does not occur until −200 mV. If the potential of the ITO coated working electrode is kept constant at a more positive potential than −200 mV, Cu and O are supposed to deposit underpotentially at the electrode surface. These electrodeposited Cu and O react to form the Cu_2O material on ITO coated surface. Cu_2O materials deposited on ITO coated glass surface for 15 min. Subsequently Ni element doped on Cu_2O/ITO/glass surface with various compositions. For this purpose, nickel solutions in different concentrations (0.0001, 0.0002, 0.0004, 0.0008, 0.001, 0.002, 0.004 and, 0.008 M) were used. Linear sweep voltammetry technique was used to dope nickel. The scanning was performed in the −800 to 600 mV potential area at a scan rate of 50 mV/s.

4.2. SEM Studies

Figure 4.1.a shows SEM image of ITO coated glass surface which belongs to working electrode in this study. Figure 4.1.b shows SEM image obtained after electrodeposition of Cu_2O semiconductor material on ITO coated glass for 15 min. Figure 4.1.c and d are

SEM images of Cu_2O material doped with Ni using 0.0001, and 0.0002 M $NiSO_4$ solution, respectively.

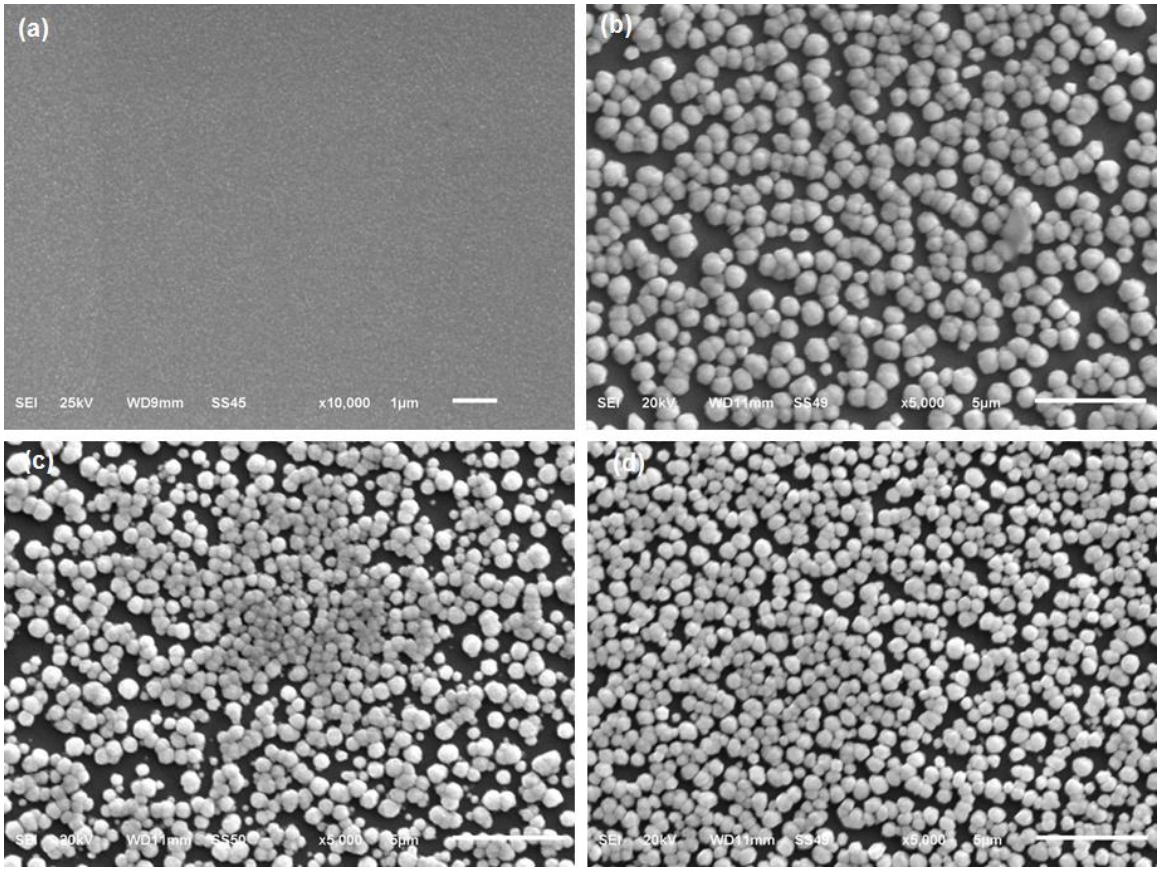

Figure 4.1. SEM image of ITO coated glass working electrode (a), SEM image of Cu_2O materials electrodeposited onto ITO coated glass surface (b), SEM images of Cu_2O materials doped with Ni using 0.0001 (c) and 0.0002 M $NiSO_4$ solution (d)

Figure 4.2.a, b, c, d, e, and f are SEM images of Cu_2O material doped with Ni using 0.0004, 0.0008, 0.001, 0.002, 0.004, and 0.008 M $NiSO_4$ solution, respectively.

In all SEM images, evenly distributed the crystals of approximately the same size are observed on the surface of the electrode. Most Cu_2O and Ni doped Cu_2O crystalline materials have a uniform shape. The conductivity of Ni is higher than Cu_2O because of Ni and Cu_2O are is a metal and semiconductor, respectively. Therefore, as the nickel concentration increases, the resolutions of SEM images increase. This result shows that the amount of nickel in the structure is increasing.

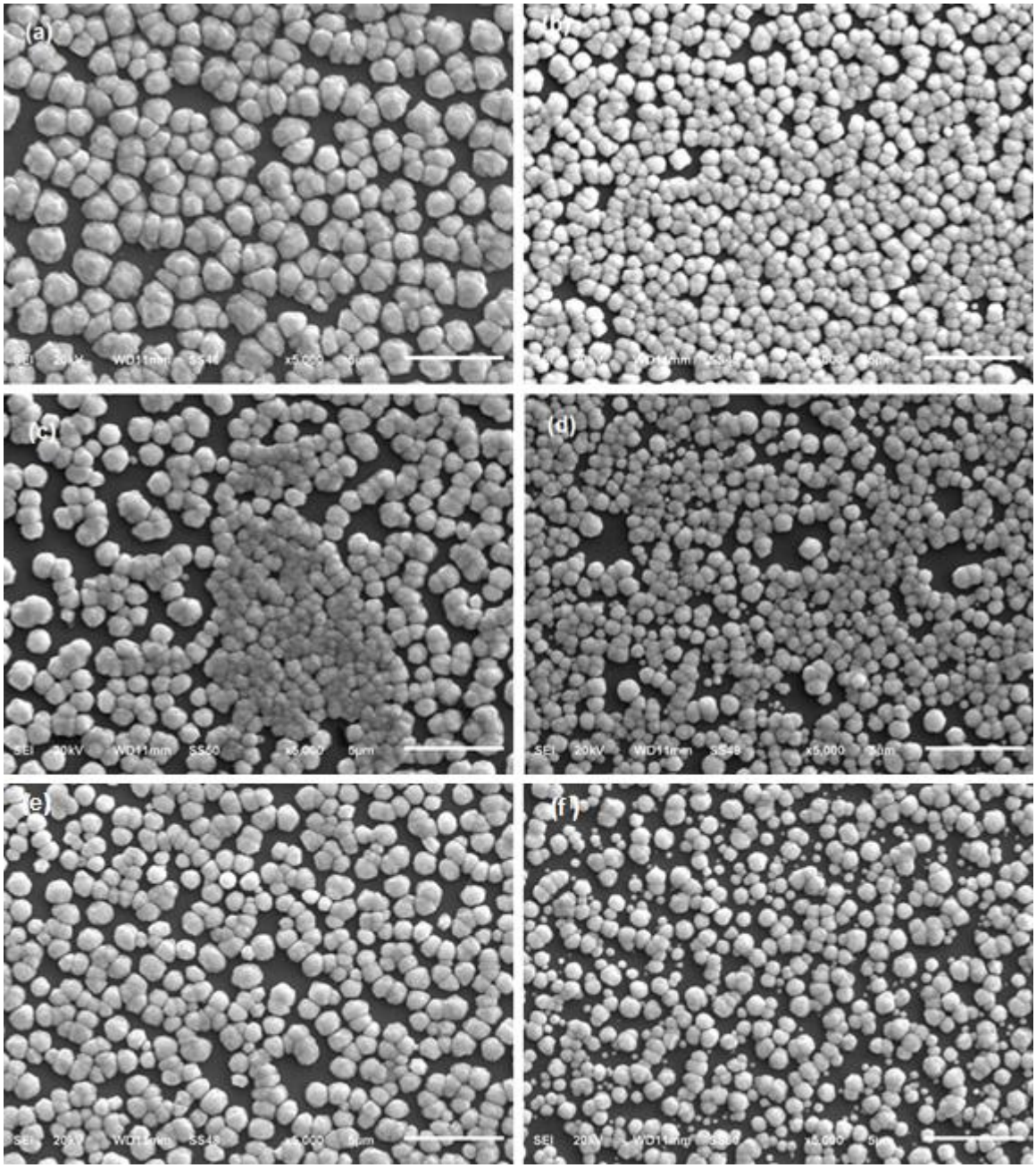

Figure 4.2. SEM images of Cu_2O materials doped with Ni using 0.0004 (a), 0.0008 (b), 0.001 (c), 0.002 (d), 0.004 (e) and 0.008 M $NiSO_4$ solution (f)

4.3. EDX Studies

The qualitative and quantitative chemical compositions of the Ni doped Cu_2O photoelectrodes were determined by the EDX. Figure 4.3 shows a EDX spectrum obtained after electrodeposition of Cu_2O material on ITO coated glass for 15 min. The EDX spectrum in Figure 4.3 clearly confirms the presence of O, Si, Cu, In, and Sn

elements. EDX analyses of different regions gave the same results. The quantitative results were 5.33% O, 7.51% Si, 39.65% Cu, 42.40% In, and 5.10% Sn elements belong to Cu_2O material and the ITO coated glass substrate used in this thesis study. This result indicates the high purity of the fabricated electrodes. The EDX peak positions were consistent with Cu_2O, and the sharp peaks of EDX indicated that the synthesized materials had a crystalline structure. The strong intensity and narrow width of the peaks indicate that the resultant products were highly crystalline in nature.

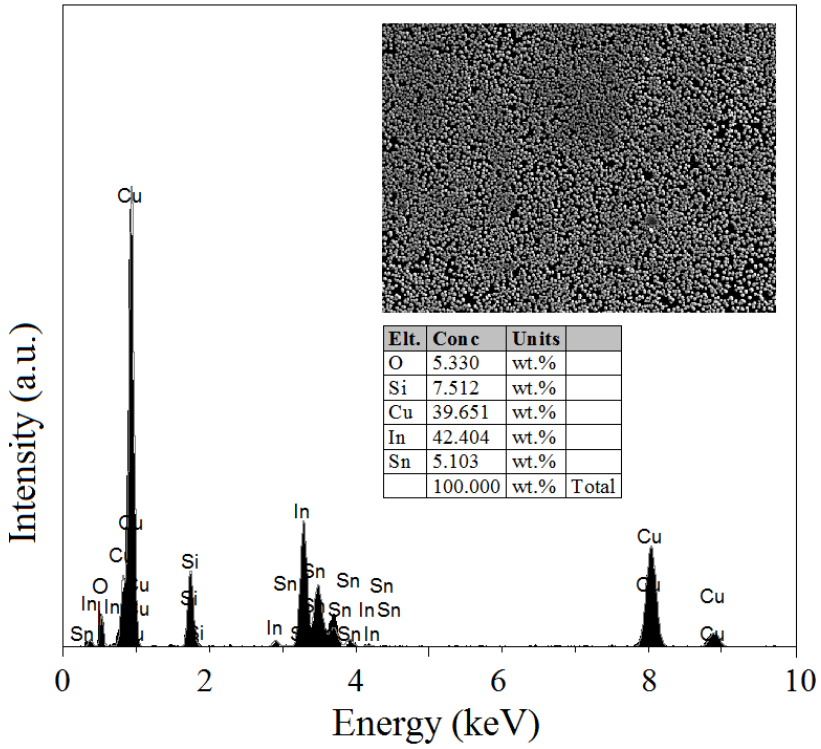

Figure 4.3. Typical EDX spectrum of undoped Cu_2O electrodeposited on ITO surface. Inset are 1000 times magnified SEM image of the material and elemental analysis collected from the entire surface

The EDX spectra provide details about the elements present in the materials and present the numerical analysis of the elements present in the samples. Thus, with the help of EDX, the doping effect and presence of dopants can be easily determined. Figure 4.4 shows a EDX spectrum of Cu_2O material doped with Ni using 0.0001 M $NiSO_4$ solution. The EDX spectrum in Figure 4.4 clearly confirms the presence of Ni, O, Si, Cu, In, and Sn elements. This means that nickel entered the structure of the Cu_2O material. In here, copper and nickel elements were only compared. The quantitative results showed 0.246%

Ni, and 99.754% Cu elements. This result indicates Ni doped Cu_2O materials. The EDX peak positions were consistent with Ni doped Cu_2O, and the sharp peaks of EDX indicated that the synthesized materials had a crystalline structure.

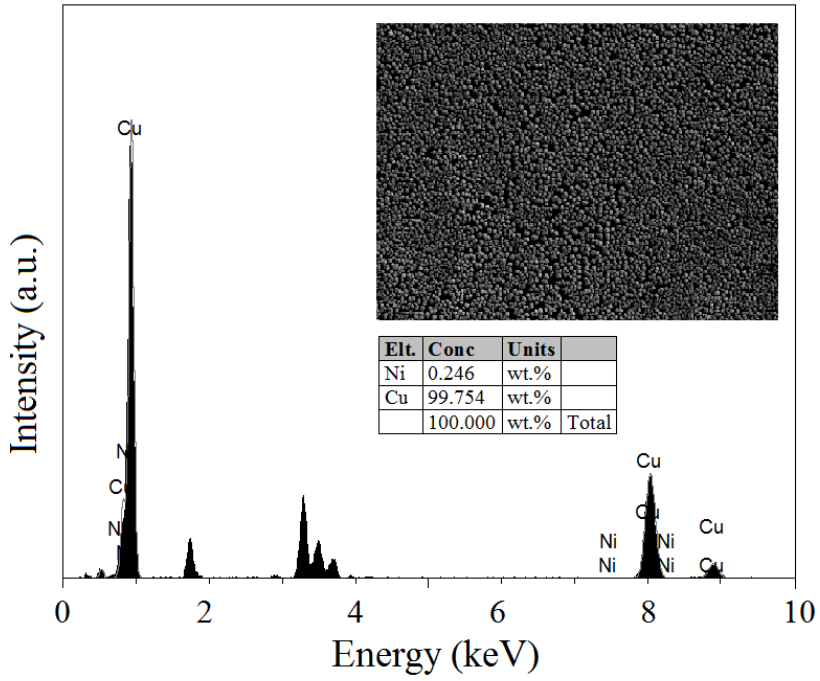

Figure 4.4. Typical EDX spectrum of Cu_2O material doped with Ni using 0.0001 M $NiSO_4$ solution. Inset are 1000 times magnified SEM image of the material and Ni and Cu elemental analysis collected from the entire surface

Figure 4.5 and 4.6 show EDX spectra of Cu_2O material doped with Ni using 0.0002 and 0.0004 M $NiSO_4$ solution, respectively. The quantitative results showed 0.352% Ni, and 99.648% Cu and 0.426% Ni, and 99.574% Cu elements, respectively. This results indicate Ni doped Cu_2O materials. The EDX peak positions were consistent with Ni doped Cu_2O, and the sharp peaks of EDX indicated that the synthesized materials had a crystalline structure.

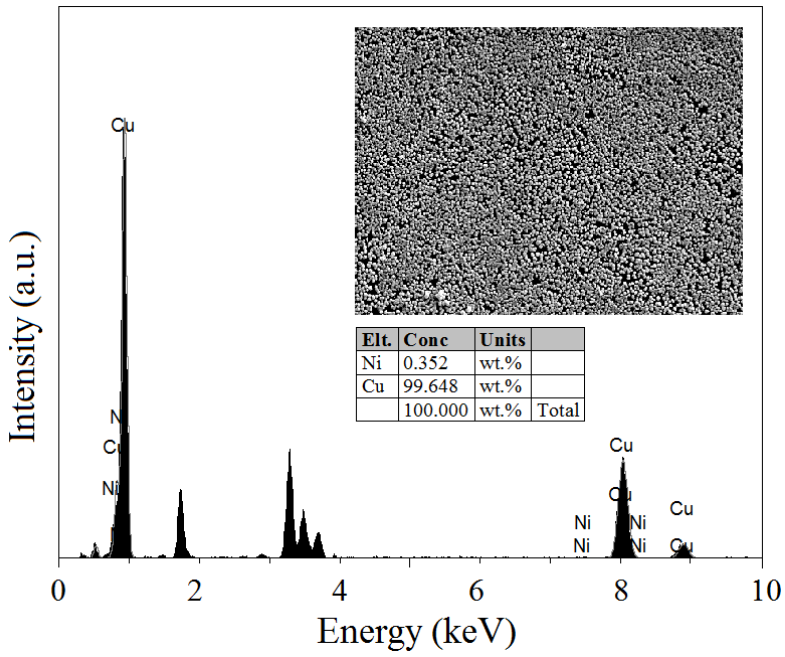

Figure 4.5. Typical EDX spectrum of Cu_2O material doped with Ni using 0.0002 M $NiSO_4$ solution. Inset are 1000 times magnified SEM image of the material and Ni and Cu elemental analysis collected from the entire surface

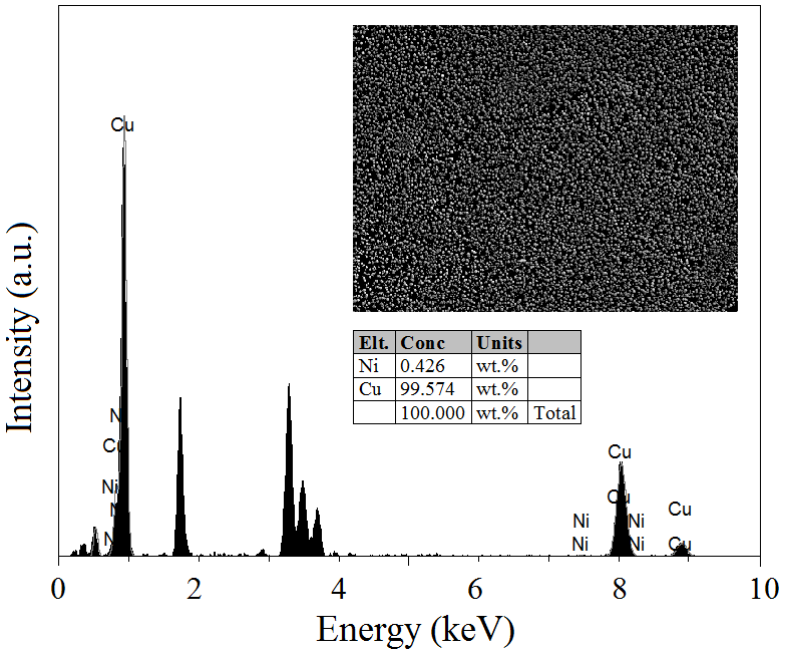

Figure 4.6. Typical EDX spectrum of Cu_2O material doped with Ni using 0.0004 M $NiSO_4$ solution. Inset are 1000 times magnified SEM image of the material and Ni and Cu elemental analysis collected from the entire surface

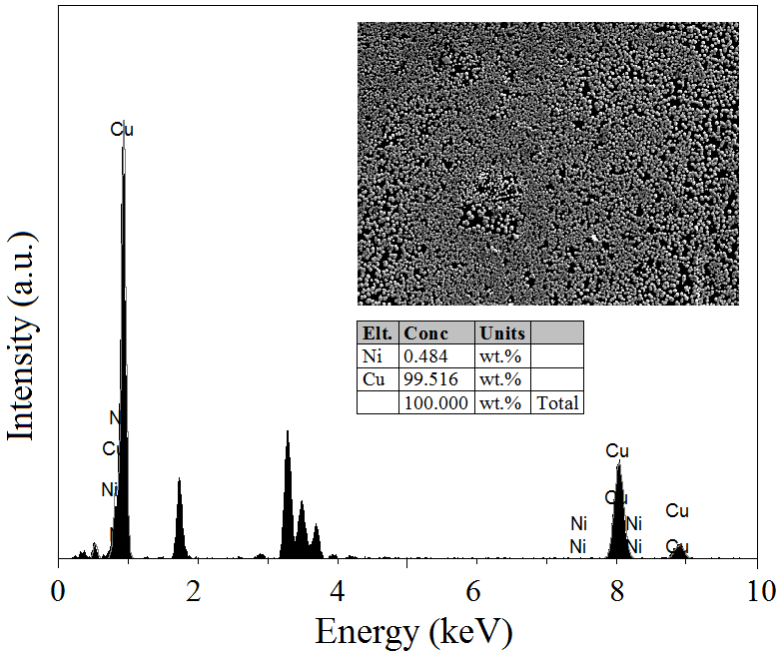

Figure 4.7. Typical EDX spectrum of Cu_2O material doped with Ni using 0.0008 M $NiSO_4$ solution. Inset are 1000 times magnified SEM image of the material and Ni and Cu elemental analysis collected from the entire surface

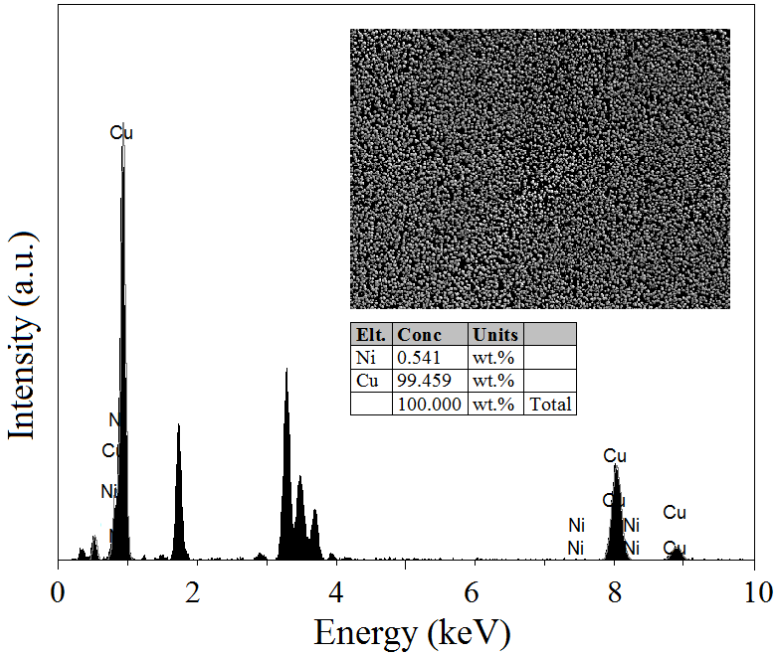

Figure 4.8. Typical EDX spectrum of Cu_2O material doped with Ni using 0.001 M $NiSO_4$ solution. Inset are 1000 times magnified SEM image of the material and Ni and Cu elemental analysis collected from the entire surface

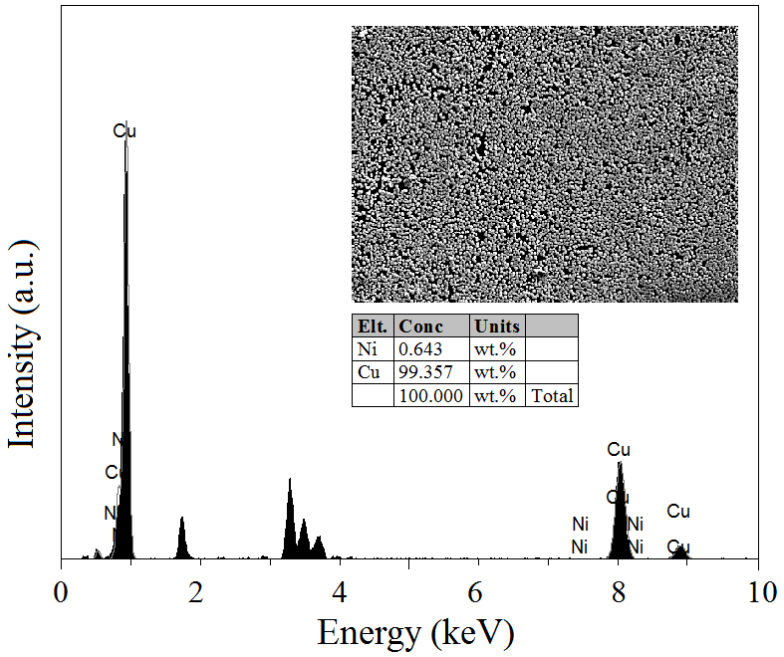

Figure 4.9. Typical EDX spectrum of Cu_2O material doped with Ni using 0.002 M $NiSO_4$ solution. Inset are 1000 times magnified SEM image of the material and Ni and Cu elemental analysis collected from the entire surface

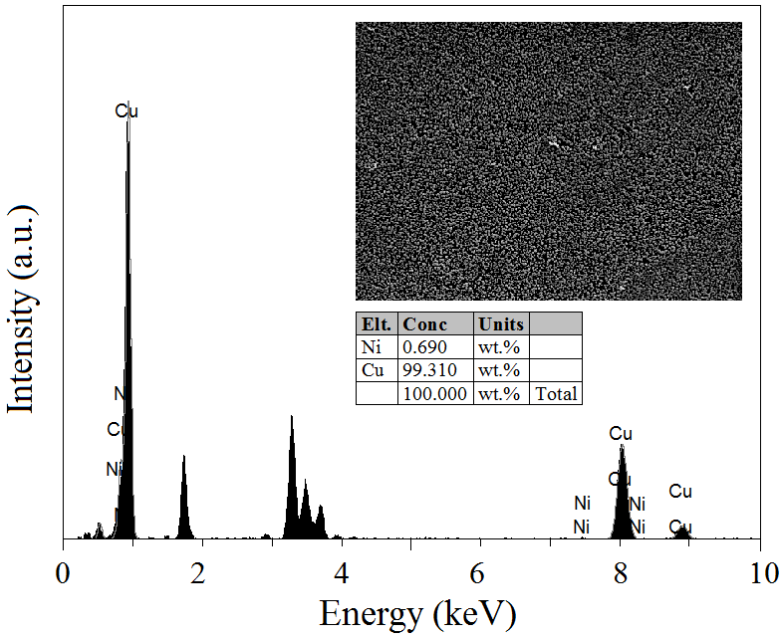

Figure 4.10. Typical EDX spectrum of Cu_2O material doped with Ni using 0.004 M $NiSO_4$ solution. Inset are 1000 times magnified SEM image of the material and Ni and Cu elemental analysis collected from the entire surface

Figure 4.7, and 4.8 show a EDX spectrum of Cu_2O material doped with Ni using 0.0008, and 0.001 M $NiSO_4$ solution, respectively. The quantitative results showed 0.484% Ni, and 99.516% Cu and 0.541% Ni, and 99.459% Cu elements, respectively.

Figure 4.9 and 4.10 show a EDX spectrum of Cu_2O material doped with Ni using 0.002 and 0.004 M $NiSO_4$ solution, respectively. The quantitative results showed 0.643% Ni, and 99.357% Cu and 0.690% Ni, and 99.310% Cu elements, respectively. This results indicate Ni doped Cu_2O materials.

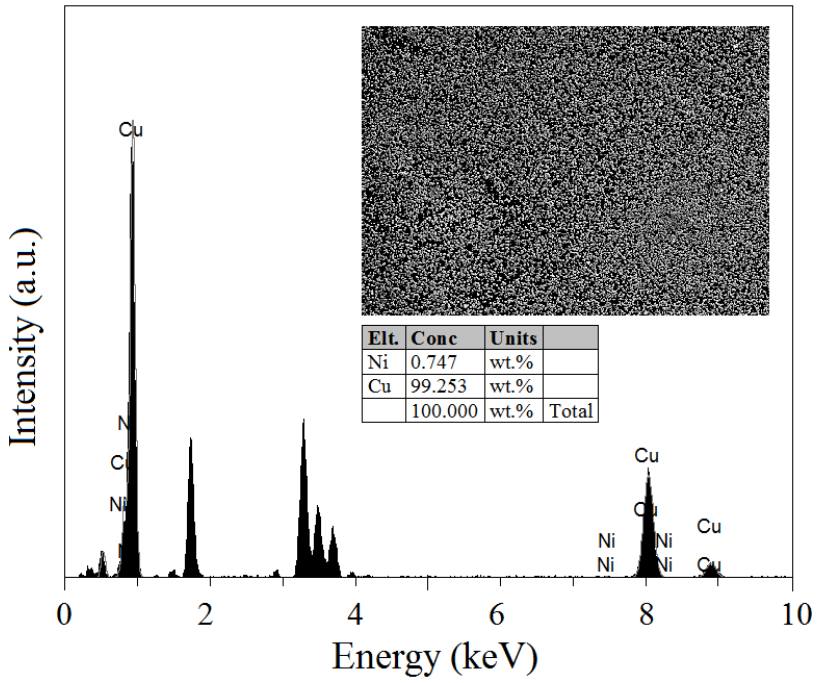

Figure 4.11. Typical EDX spectrum of Cu_2O material doped with Ni using 0.008 M $NiSO_4$ solution. Inset are 1000 times magnified SEM image of the material and Ni and Cu elemental analysis collected from the entire surface

Figure 4.11 shows a EDX spectrum of Cu_2O material doped with Ni using 0.008 M $NiSO_4$ solution. The quantitative result showed a chemical composition consisting of 0.747% Ni, and 99.253% Cu elements. This result indicates Ni doped Cu_2O materials. The EDX peak positions were consistent with Ni doped Cu_2O, and the sharp peaks of EDX indicated that the synthesized materials had a crystalline structure. Thus, with the help of EDX, the nickel doping effect and presence of dopants were determined. The

amount of Ni in the materials has been found to vary between 0.246 and 0.747 wt.%. As the nickel concentration increased, the nickel amount of Cu_2O materials increased.

4.4. XRD Studies

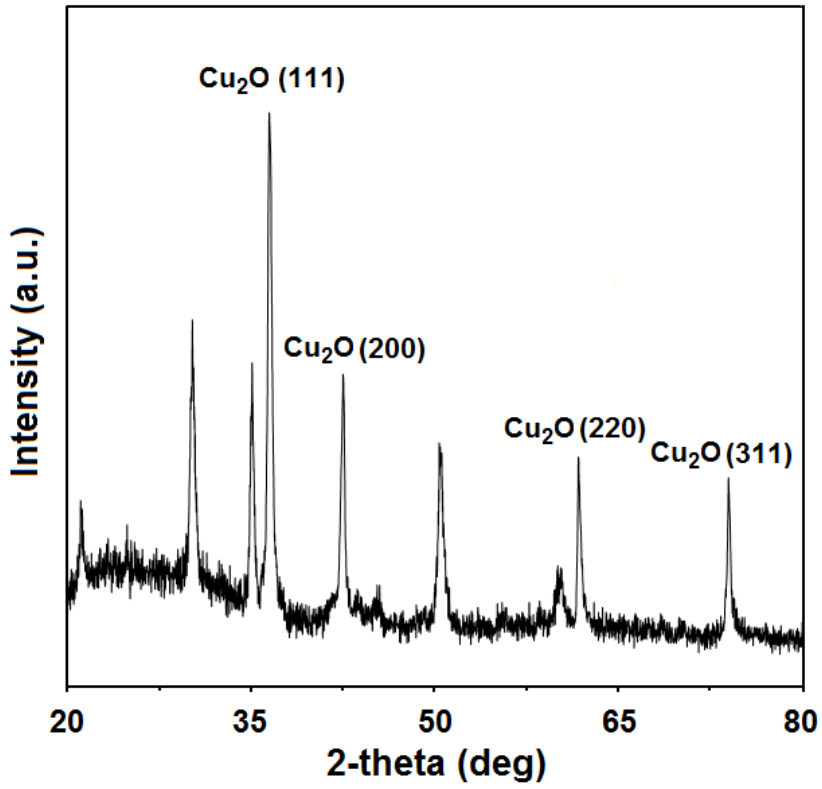

Figure 4.12. Typical XRD diffractogram of Cu_2O materials doped with Ni using 0.008 M $NiSO_4$ solution

Figure 4.12 is XRD diffractograms of Cu_2O materials doped with Ni using 0.008 M $NiSO_4$ solution. The XRD diffractogram of nickel doped copper (I) oxide consists of a strong diffraction peak at 36.6° arising from (1 1 1) reflections from Cu_2O. The weaker diffractions at 42.5°, 61.7°, and 73.9° corresponds to (2 0 0), (2 2 0), and (3 1 1) reflections of Cu_2O. The other peaks belong to ITO coated glass which belongs to working electrode in this study. The other XRD diffractograms of Cu_2O and Ni doped Cu_2O at different amounts of nickel doping are similar to Figure 4.12. No peaks belong to elemental nickel or any type of nickel was detected in XRD patterns. Ni presence was not observed in the XRD pattern because the amount of Ni in the structure is very small. XRD results indicate that highly crystalline materials of Ni doped Cu_2O.

4.5. Absorbance and Band Gap Studies

Absorbance spectrum of Cu_2O materials doped with Ni using 0.008 M $NiSO_4$ solution is shown in Figure 4.13. In here, one absorption band in the UV-Vis region observed. The absorption edge measured for photoelectrodes are 580 nm. The fundamental absorption edges at 580 nm correspond to copper (I) oxide. The other absorbance spectrums of Cu_2O and Ni doped Cu_2O materials at different amounts of nickel doping are similar to Figure 4.14.

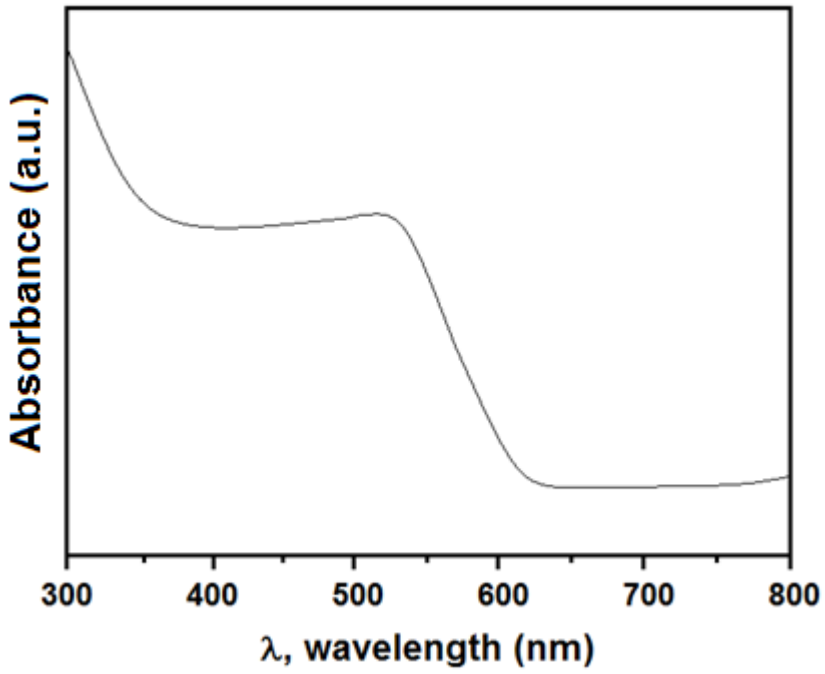

Figure 4.13. Absorbance spectrum of Cu_2O materials doped with Ni using 0.008 M $NiSO_4$ solution

For all the semiconductors, the widely used method of plotting $(\alpha hv)^2$ versus the energy hv is adopted to determine the band gap of the materials. The Eg can thus be estimated from a plot of $(\alpha hv)^2$ versus the photon energy hv. The band gap of the materials electrodeposited onto ITO coated glass was found to be Eg = 2.14 eV.

4.6. PEC Studies

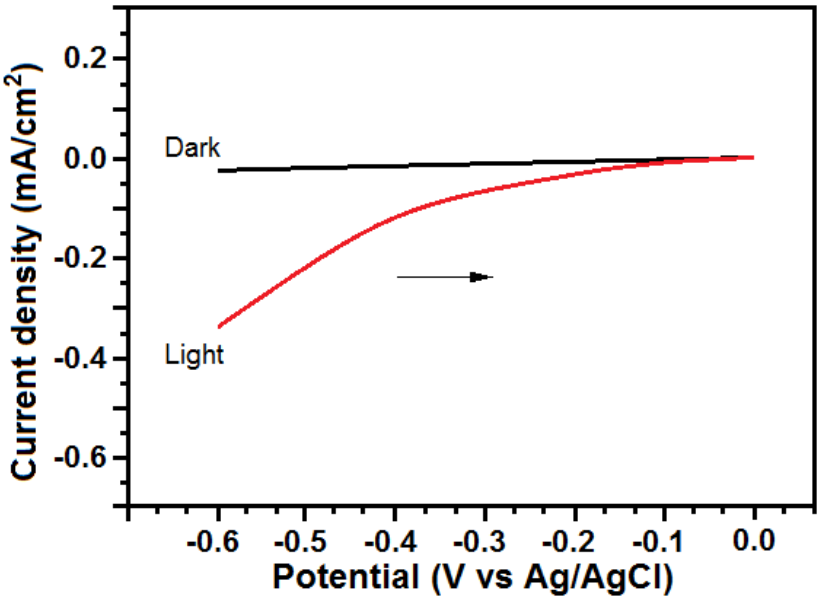

Figure 4.14. Linear sweep voltammograms of undoped Cu_2O semiconductor photoelectrodes in 0.1 M Na_2SO_4

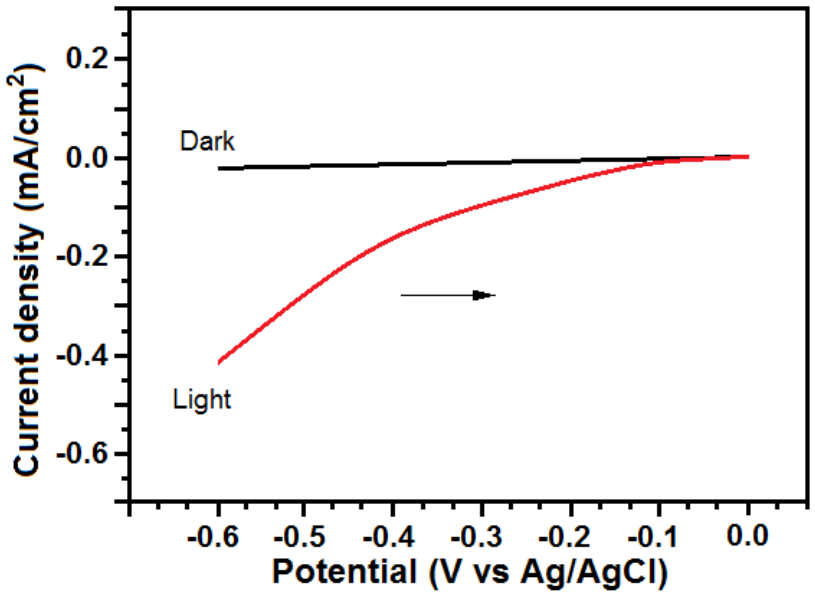

Figure 4.15. Linear sweep voltammograms of Cu_2O materials doped with Ni using 0.0001 M $NiSO_4$ solution in 0.1 M Na_2SO_4

Figure 4.14-4.22 shows the effect of nickel doping on the light and dark currents of Ni doped Cu_2O semiconductor photoelectrodes. Figure 4.14 shows linear sweep

voltammograms of Cu_2O semiconductor photoelectrodes electrodeposited for 15 min in dark and light. This linear sweep voltammogram exhibited a photocathodic behavior due to the p-type nature of the Cu_2O semiconductors.

Figure 4.15 shows linear sweep voltammograms of Cu_2O photoelectrodes doped with Ni using 0.0001 M $NiSO_4$ solution. It also exhibited a photocathodic behavior. The photocurrents increased with nickel dopping.

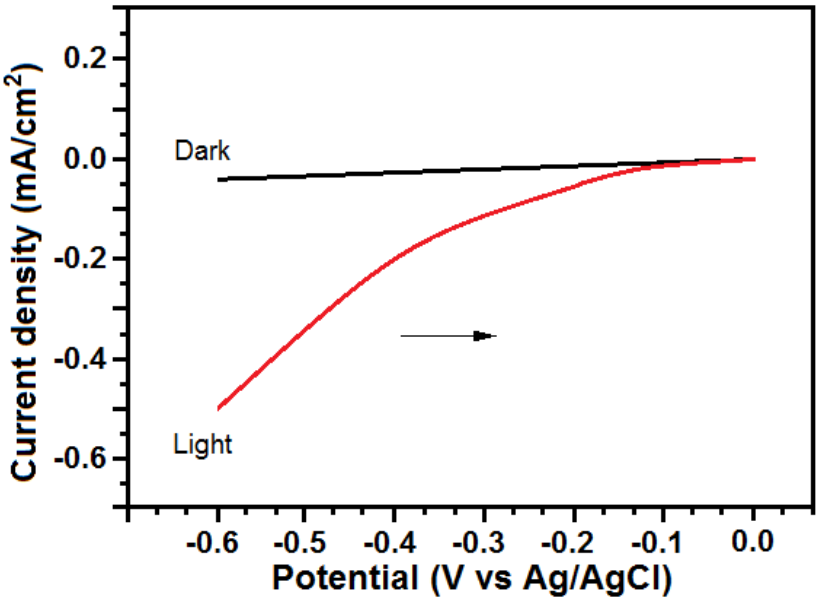

Figure 4.16. Linear sweep voltammograms of Cu_2O materials doped with Ni using 0.0002 M $NiSO_4$ solution in 0.1 M Na_2SO_4

Figure 4.16 exhibits linear sweep voltammograms of Cu_2O photoelectrodes doped with Ni using 0.0002 M $NiSO_4$ solution. As the amount of nickel doping increased, the photocurrents of Ni doped Cu_2O photoelectrodes increased. The Cu_2O photoelectrodes doped with Ni using 0.0002 M $NiSO_4$ solution exhibit the highest photocurrents between the investigated all the materials.

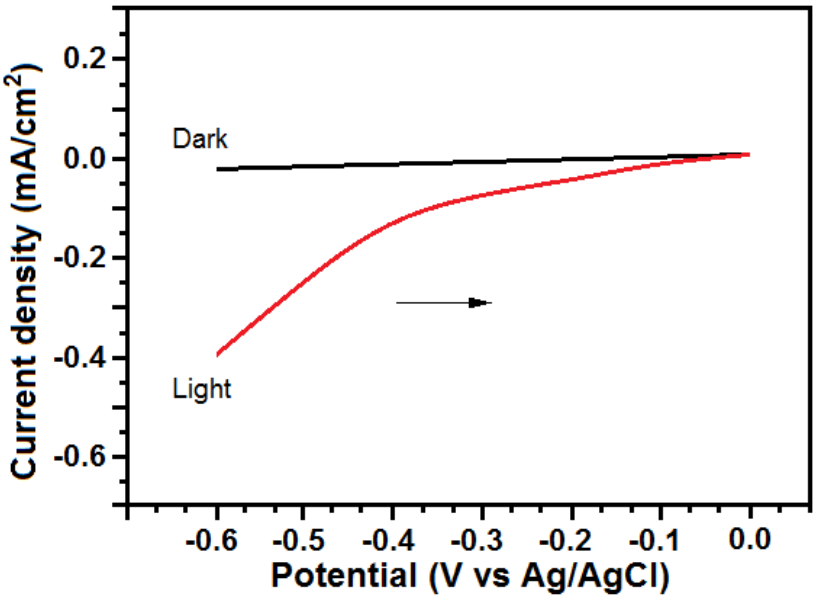

Figure 4.17. Linear sweep voltammograms of Cu_2O materials doped with Ni using 0.0004 M $NiSO_4$ solution in 0.1 M Na_2SO_4

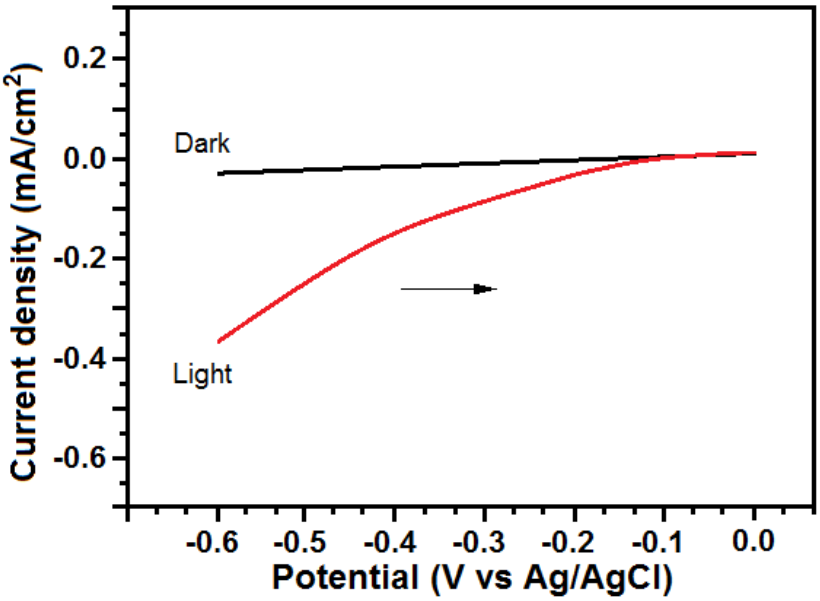

Figure 4.18. Linear sweep voltammograms of Cu_2O materials doped with Ni using 0.0008 M $NiSO_4$ solution in 0.1 M Na_2SO_4

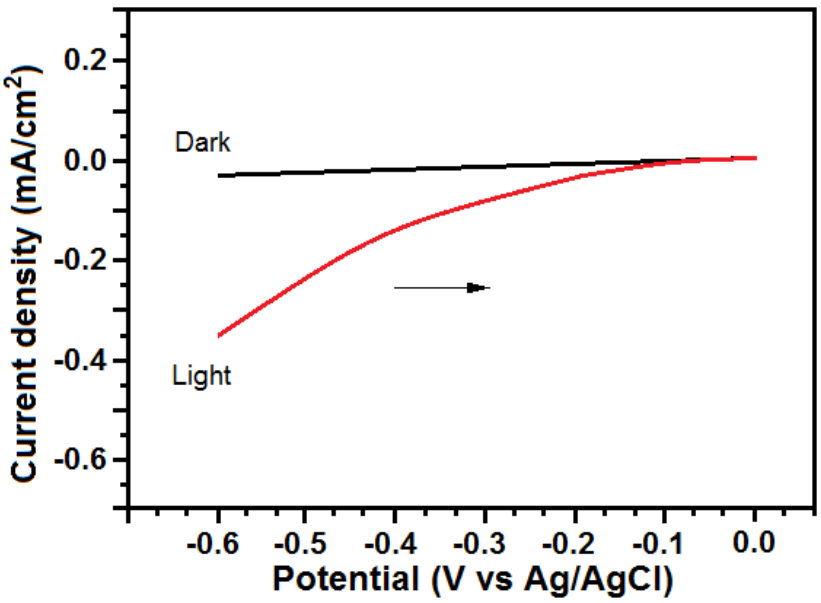

Figure 4.19. Linear sweep voltammograms of Cu_2O materials doped with Ni using 0.001 M $NiSO_4$ solution in 0.1 M Na_2SO_4

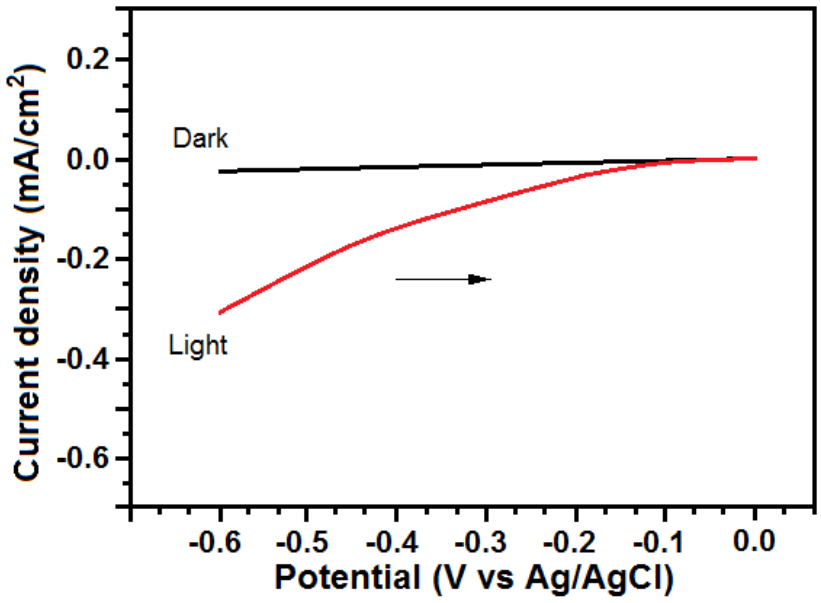

Figure 4.20. Linear sweep voltammograms of Cu_2O materials doped with Ni using 0.002 M $NiSO_4$ solution in 0.1 M Na_2SO_4

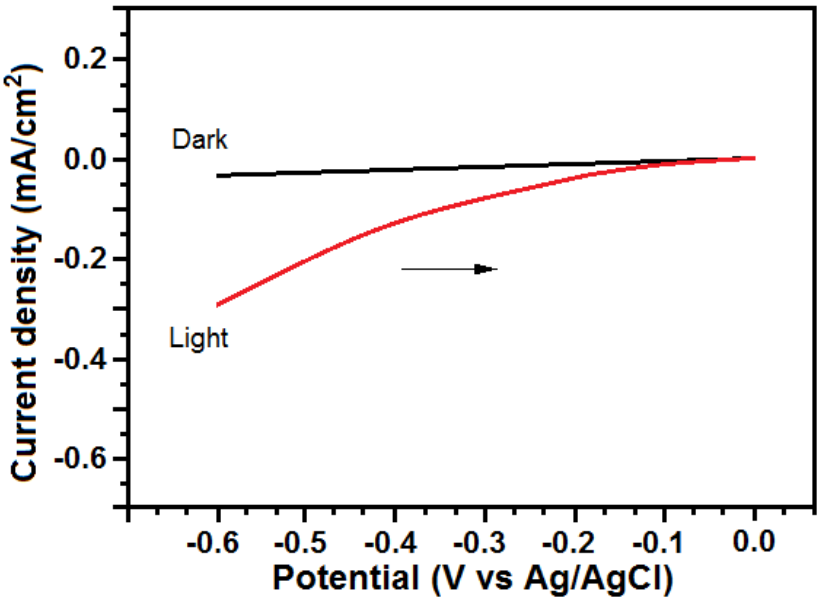

Figure 4.21. Linear sweep voltammograms of Cu_2O materials doped with Ni using 0.004 M $NiSO_4$ solution in 0.1 M Na_2SO_4

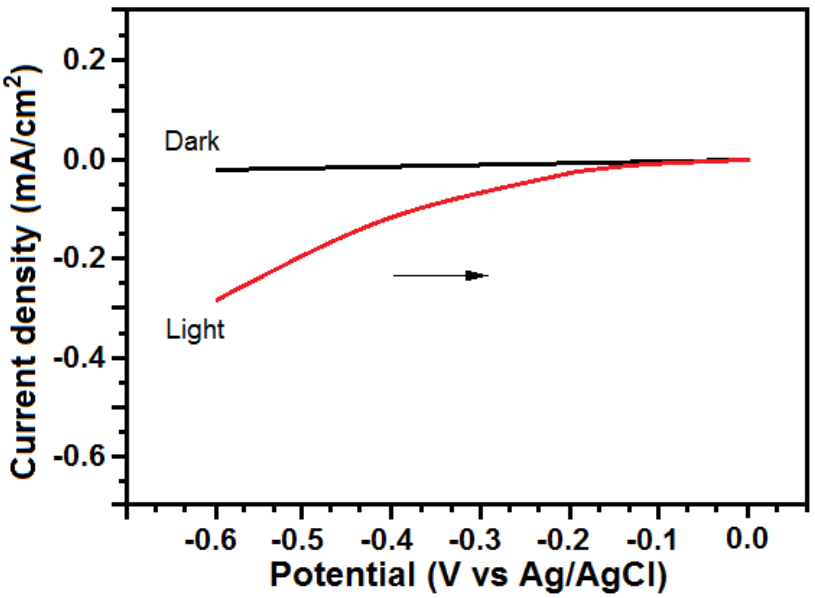

Figure 4.22. Linear sweep voltammograms of Cu_2O materials doped with Ni using 0.008 M $NiSO_4$ solution in 0.1 M Na_2SO_4

Figure 4.17, 18, 19, 20, 21, and 22 exhibit linear sweep voltammograms of Cu_2O photoelectrodes doped with Ni using 0.0004, 0.0008, 0.001, 0.002, 0.004, 0.008 M $NiSO_4$ solution, respectively. As the amount of nickel doping increased, the photocurrents of Ni doped Cu_2O photoelectrodes decreased. This may be due to the increased bending of Ni

doped Cu_2O photoelectrodes for the amounts of nickel doping, which may reduce the effective area for surface reactions leading to lower photocurrents. It also shows that the material structure turned from a semiconductor character to a metal character. All the linear sweep voltammograms showed a photocathodic behavior due to the p-type nature of the Ni doped Cu_2O semiconductors.

Figure 4.23 illustrates the current density under sun light for the corresponding copper (I) oxide and nickel doped copper (I) oxide photoelectrodes. Herein, the effect of amount of the nickel doping on the photocurrents of Cu_2O photoactive semiconductor materials is exhibited.

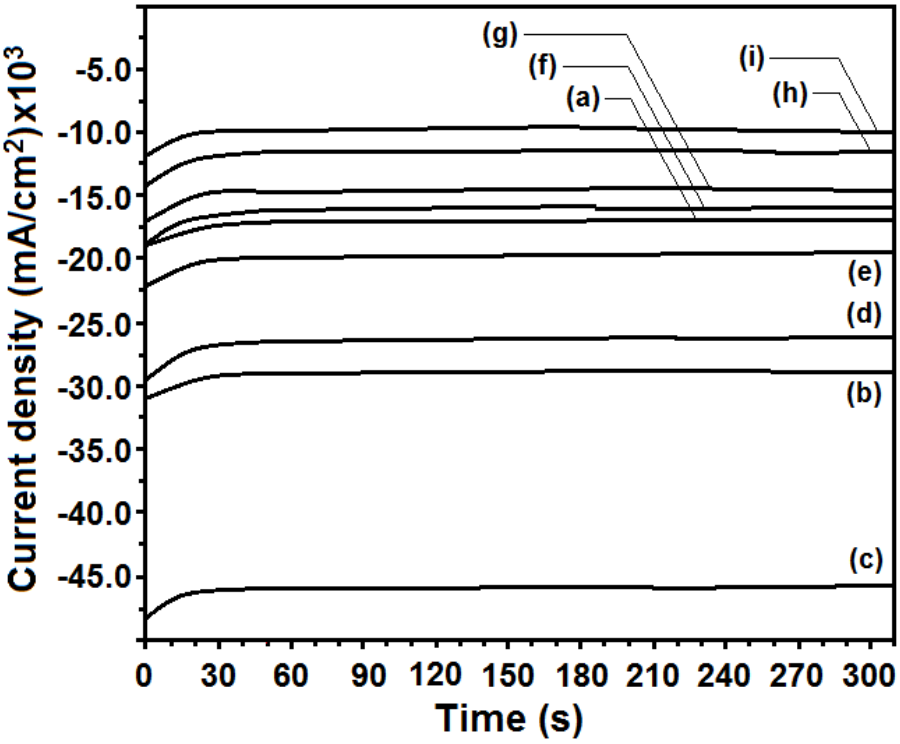

Figure 4.23. Photocurrent responses of undoped and Ni doped Cu_2O photoelectrodes under light illumination in 0.1 M Na_2SO_4. Current density of the photoelectrodes; (a) undoped Cu_2O, Cu_2O materials doped with Ni using 0.0001 (b), 0.0002 (c), 0.0004 (d), 0.0008 (e) 0.001 (f), 0.002 (g), 0.004 (h), and 0.008 M $NiSO_4$ solution (i)

Figure 4.23.a shows chronoamperogram of Cu_2O semiconductor photoelectrodes electrodeposited for 15 min under light. Figure 4.23.b, and c exhibit chronoamperograms of Cu_2O photoelectrodes doped with Ni using 0.0001 and 0.0002 M $NiSO_4$ solution, respectively. As the amount of nickel doping increased, the current density of Ni doped

Cu_2O semiconductor photoelectrodes increased. The Cu_2O photoelectrodes doped with Ni using 0.0002 M $NiSO_4$ solution (Figure 4.23.c) exhibit the highest current density between the investigated all materials. Figure 4.23.d, e, f, g, h, and i show chronoamperograms of Cu_2O photoelectrodes doped with Ni using 0.0004, 0.0008, 0.001, 0.002, 0.004, and 0.008 M $NiSO_4$ solution, respectively. As the amount of nickel doping increased, the current density of Ni doped Cu_2O photoelectrodes decreased. Cu_2O photoelectrodes doped with Ni using 0.0001, 0.0002, 0.0004, and 0.0008 M $NiSO_4$ solution (Figure 4.23.b, c, d, e) showed better the current density than undoped Cu_2O semiconductor photoelectrodes (Figure 4.23.a).

The trends for different the amounts of nickel doping in the current density (Figure 4.23) confirm the observed trends in Figure 4.14-4.22. As shown in Figure 4.23, undoped Cu_2O and Ni doped Cu_2O photoelectrodes exhibit good stability and switching behavior for different the amounts of nickel doping.

5. CONCLUSIONS AND RECOMMENDATIONS

This thesis study reports on the synthesis of homogeneous Ni doped Cu_2O materials with various compositions using electrochemical technique. The UPD potential for Cu were determined by cyclic voltammetric measurements. In order to determine a deposition potential of the Cu_2O from the solution, the cyclic voltammetric measurements of copper were also recorded at the UPD region in the aqueous medium. Cu_2O materials deposited on ITO coated glass surface for 15 min. Subsequently Ni element doped on Cu_2O/ITO/glass surface with various compositions. For this purpose, nickel solutions in different concentrations were used. Linear sweep voltammetry technique was used to dope nickel.

The EDX spectra provide details about the elements present in the materials and present the numerical analysis of the elements present in the samples. The EDX spectra confirm the presence of Ni, O, Si, Cu, In, and Sn elements. This means that nickel entered the structure of the Cu_2O material. The results indicate Ni doped Cu_2O materials. The EDX peak positions were consistent with Ni doped Cu_2O, and the sharp peaks of EDX indicated that the synthesized materials had a crystalline structure. As the nickel concentration increased, the nickel amount of Cu_2O materials increased.

All SEM images, evenly distributed the crystals of approximately the same size are observed on the surface of the electrode. Most Cu_2O and Ni doped Cu_2O crystalline materials have a uniform shape. The conductivity of Ni is higher than Cu_2O because of Ni and Cu_2O are is a metal and semiconductor, respectively. Therefore, as the nickel concentration increases, the resolutions of SEM images increase. This is an indication that the amount of nickel in the structure is increasing.

The XRD diffractograms of Ni doped copper (I) oxide consists of a strong diffraction peak arising from (1 1 1) reflections from Cu_2O. All the XRD diffractograms of Cu_2O

and Ni doped Cu_2O at different amounts of nickel doping are similar. No peaks belong to elemental nickel or any type of nickel was detected in XRD patterns. Ni presence was not observed in the XRD pattern because the amount of Ni in the structure is very small. XRD results indicate that highly crystalline materials of Ni doped Cu_2O.

In absorbance spectrum of Cu_2O and Ni doped Cu_2O materials, one absorption band in the UV-Vis region observed. The absorption edge measured for photoelectrodes are 580 nm. The other absorbance spectrums of Cu_2O and Ni doped Cu_2O materials at amounts of nickel doping are similar. The band gap of the materials electrodeposited onto ITO coated glass was found to be Eg = 2.14 eV.

All the linear sweep voltammograms showed a photocathodic behavior due to the p-type nature of the Ni doped Cu_2O semiconductors. As the amount of nickel doping increased, the photocurrents of Ni doped Cu_2O photoelectrodes decreased. This may be due to the increased bending of Ni doped Cu_2O photoelectrodes for the amounts of nickel doping, which may reduce the effective area for surface reactions leading to lower photocurrents. It also shows that the material structure turned from a semiconductor character to a metal character.

The current density under sun light for the corresponding copper (I) oxide and nickel doped copper (I) oxide photoelectrodes showed that as the amount of nickel doping increased, the current density of Ni doped Cu_2O semiconductor photoelectrodes increased. The Cu_2O photoelectrodes doped with Ni using 0.0002 M $NiSO_4$ solution exhibit the highest current density between the investigated all materials. Cu_2O photoelectrodes doped with Ni using 0.0001, 0.0002, 0.0004, and 0.0008 M $NiSO_4$ solution showed better the current density than undoped Cu_2O photoelectrodes. The undoped Cu_2O and Ni doped Cu_2O photoelectrodes exhibit good stability and switching behavior for different the amounts of nickel doping. Ni doped Cu_2O photoelectrodes are suggested as a competitive candidate for advanced photoelectrochemical detection, maybe for the extended field of photoelectrochemical water splitting and other solar photovoltaic technologies.

REFERENCES

Ahmed A, Gajbhiye NS (2010) Room temperature ferromagnetism in Mn, Ni and Co ions doped Cu_2O nanorods. Journal of Solid State Chemistry 183: 3100-3104

Ahn KS, Shet S, Deutsch T, Jiang CS, Yan Y, Al-Jassim M, Turner J (2008) Enhancement of photoelectrochemical response by aligned nanorods in ZnO thin films. Journal of Power Sources 176: 387-392

Aho AE (1956) Geology and genesis of ultrabasic nickel-copper-pyrrhotite deposits at the Pacific Nickel property, southwestern British Columbia. Economic Geology 51: 444-481

Aissa MAB, Tremblay B Andrieux-Ledier A, Maisonhaute E, Raouafi N, Courty A (2015) Copper nanoparticles of well-controlled size and shape: a new advance in synthesis and self-organization. Nanoscale 7: 3189-3195

Aldana J, Lavelle N, Wang Y, Peng X (2005) Size-dependent dissociation pH of thiolate ligands from cadmium chalcogenide nanocrystals. Journal of the American Chemical Society 127: 2496-2504

Alivisatos AP, Gu W, Larabell C (2005) Quantum dots as cellular probes. Annu. Rev. Biomed. Eng. 7: 55-76

Amin G, Willander, PM (2012) ZnO and CuO Nanostructures Low Temperature Growth, Characterization, their Optoelectronic and Sensing Applications. Department of Science and Technology, Physics and Electronics, Sweden

Andersen A, Berge SR, Engeland A, Norseth T (1997) Exposure to nickel compounds and smoking in relation to incidence of lung and nasal cancer among nickel refinery workers. Occupational Health and Industrial Medicine 1(36): 38-39

Barbour EK, Sabra AH, Bianu EG, Jaber LS, Shaib HA (2009) Oppositional dynamics of organic versus inorganic contaminants in oysters following an oil spill. Journal of Coastal Research 1: 864-869

Bard AJ (1979) Photoelectrochemistry and heterogeneous photo-catalysis at semiconductors. Journal of Photochemistry 10(1): 59-75

Basith NM, Vijaya JJ, Kennedy LJ, Bououdina M (2014) Structural, morphological, optical, and magnetic properties of Ni-doped CuO nanostructures prepared by a rapid microwave combustion method. Materials Science in Semiconductor Processing 17: 110-118

Beattie SD, Dahn JR (2003) Single bath, pulsed electrodeposition of copper-tin alloy negative electrodes for lithium-ion batteries. Journal of The Electrochemical Society 150(7): A894-A898

Brattain WH, Garrett CGB (1955) Experiments on the interface between germanium and an electrolyte. Bell Labs Technical Journal 34(1): 129-176

Castellar Ramos MI, Osorio Tamayo JC (2012) Estado del arte de la fotocatálisis solar como técnica para la remoción de efluentes químicos provenientes de laboratorios

Cataldo DA, Garland TR, Wildung RE, Drucker H (1978) Nickel in plants. Plant Physiology 62(4): 566-570

Chatterjee AP, Mukhopadhyay AK, Chakraborty AK, Sasmal RN, Lahiri SK (1991) Electrodeposition and characterisation of cuprous oxide films. Materials Letters 11(10-12): 358-362

Chigane M, Ishikawa M (1994) Enhanced electrochromic property of nickel hydroxide thin films prepared by anodic deposition. Journal of The Electrochemical Society 141(12): 3439-3443

Chmaissem O, Jorgensen JD, Short S, Knizhnik A, Eckstein Y, Shaked H (1999) Scaling of transition temperature and CuO plane buckling in a high-temperature superconductor. Nature 397(6714): 45-48

Coe S, Woo WK, Bawendi M, Bulović V (2002) Electroluminescence from single monolayers of nanocrystals in molecular organic devices. Nature 420(6917): 800-803

Deki S, Akamatsu K, Yano T, Mizuhata M, Kajinami A (1998) Preparation and characterization of copper (I) oxide nanoparticles dispersed in a polymer matrix. Journal of Materials Chemistry 8(8): 1865-1868

Diwan BA, Kasprzak KS, Rice JM (1992) Transplacental carcinogenic effects of nickel (II) acetate in the renal cortex, renal pelvis and adenohypophysis in F3447/NCr rats. Carcinogenesis 13(8): 1351-1357

Du F, Chen QY, Wang YH (2017) Effect of annealing process on the heterostructure CuO/Cu_2O as a highly efficient photocathode for photoelectrochemical water reduction. Journal of Physics and Chemistry of Solids 104: 139-144

Erdoğan İY, Demir U (2009) Synthesis and characterization of Sb_2Te_3 nanofilms via electrochemical co-deposition method. Journal of Electroanalytical Chemistry 633: 253-258

Erdoğan İY, Oznuluer T, Bulbul F, Demir U (2009) Characterization of size-quantized PbTe thin films synthesized by an electrochemical co-deposition method. Thin Solid Films 517: 5419-5424

Erdoğan İY, Demir U (2011) Orientation-controlled synthesis and characterization of Bi_2Te_3 nanofilms, and nanowires via electrochemical co-deposition. Electrochimica Acta 56: 2385-2393

Fan H, Yang L, Hua W, Wu X, Wu Z, Xie S, Zou B (2003) Controlled synthesis of monodispersed CuO nanocrystals. Nanotechnology 15(1): 37-38

Finn BS (1980) Thermoelectricity. Advances in Electronics and Electron Physics 50: 175-240

Firdous A, Singh D, Ahmad MM (2013) Electrical and optical studies of pure and Ni-doped CdS quantum dots. Applied Nanoscience 3(1): 13-18

Fujishima A, Honda K (1972) Electrochemical photolysis of water at a semiconductor electrode. Nature 238(5358): 37-38

Georgieva V, Ristov M (2002) Electrodeposited cuprous oxide on indium tin oxide for solar applications. Solar Energy Materials and Solar Cells 73(1): 67-73

Gerischer H, Lübke M (1988) On the Etching of Silicon by Oxidants in Ammonium Fluoride Solutions A Mechanistic Study. Journal of The Electrochemical Society 135(11): 2782-2786

Goodridge F, King CJH (1974) Technique of electroorganic synthesis. Part 1, weinberg NL, Ed, wiley, NewYork

Heyrovsky J (1922) Elektrolysa se rtufovoukapkoyoukathodou. Chem. Listy 16: 256-264

Huang LS, Yang SG, Li T, Gu BX, Du YW, Lu YN, Shi SZ (2004) Preparation of large-scale cupric oxide nanowires by thermal evaporation method. Journal of Crystal Growth 260(1): 130-135

Humayun Q, Kashif M, Hashim U (2013) Area-selective ZnO thin film deposition on variable microgap electrodes and their impact on UV sensing. Journal of Nanomaterials 42: 112-113

Ibl N, Vogt H (1981) Inorganic electrosynthesis. In Comprehensive treatise of electrochemistry (pp. 167-250) Springer US

Ishihara T, Higuchi M, Takagi T, Ito M, Nishiguchi H, Takita Y (1998) Preparation of CuO thin films on porous $BaTiO_3$ by self-assembled multibilayer film formation and application as a CO_2 sensor. Journal of Materials Chemistry 8(9): 2037-2042

Jiang Y, Meng XM, Liu J, Hong ZR, Lee CS, Lee ST (2003) ZnS nanowires with wurtzite polytype modulated structure. Advanced Materials 15(14): 1195-1198

Jiang Y, Zhang WJ, Jie JS, Meng XM, Zapien JA, Lee ST (2006) Homoepitaxial growth and lasing properties of ZnS nanowire and nanoribbon arrays. Advanced Materials 18(12): 1527-1532

Katti VR, Debnath AK, Muthe KP, Kaur M, Dua AK, Gadkari SC, Sahni VC (2003) Mechanism of drifts in H_2S sensing properties of SnO_2: CuO composite thin film sensors prepared by thermal evaporation. Sensors and Actuators B: Chemical 96(1): 245-252

Kikuchi N, Tonooka K (2005) Electrical and structural properties of Ni-doped Cu_2O films prepared by pulsed laser deposition. Thin Solid Films 486(1): 33-37

Kikuchi N, Tonooka K, Kusano E (2006) Mechanisms of carrier generation and transport in Ni-doped Cu_2O. Vacuum 80(7): 756-760

Koval CA, Howard JN (1992) Electron transfer at semiconductor electrode-liquid electrolyte interfaces. Chemical Reviews 92(3): 411-433

Kumar RV, Mastai Y, Diamant Y, Gedanken A (2001) Sonochemical synthesis of amorphous Cu and nanocrystalline Cu_2O embedded in a polyaniline matrix. Journal of Materials Chemistry 11(4): 1209-1213

Kumar S, Nann T (2006) Shape control of II–VI semiconductor nanomaterials. Small 2(3): 316-329

Laik B, Poizot P, Tarascon JM (2002) The Electrochemical Quartz Crystal Microbalance as a Means for Studying the Reactivity of Cu_2O toward Lithium. Journal of The Electrochemical Society 149(3): A251-A255

Lee S, Choi SS, Li SA, Eastman JA (1999) Measuring thermal conductivity of fluids containing oxide nanoparticles. Journal of Heat transfer 121(2): 280-289

Li G, Dimitrijevic NM, Chen L, Rajh T, Gray KA (2008) Role of surface/interfacial Cu^{2+} sites in the photocatalytic activity of coupled $CuO{-}TiO_2$ nanocomposites. The Journal of Physical Chemistry C 112(48): 19040-19044

Liang D, Han G, Zhang Y, Rao S, Lu S, Wang H, Xiang Y (2016) Efficient H_2 production in a microbial photoelectrochemical cell with a composite Cu_2O/NiO_x photocathode under visible light. Applied Energy 168: 544-549

Liang YQ, Gao ZH, Cui ZD, Zhu SL, Li ZY, Yang X. J. (2014). Photocatalytic performance of Ag nanoparticles modified ZnO microplates prepared by one-step method. Current Nanoscience 10(3): 389-393

Lu Q, Gao F, Komarneni S (2006) Cellulose-directed growth of selenium nanobelts in solution. Chemistry of Materials 18(1): 159-163

Ma QB, Hofmann JP, Litke A, Hensen EJ (2015) Cu_2O photoelectrodes for solar water splitting: tuning photoelectrochemical performance by controlled faceting. Solar Energy Materials and Solar Cells 141: 178-186

Mageshwari K, Sathyamoorthy R (2013) Flower-shaped CuO nanostructures: synthesis, characterization and antimicrobial activity. Journal of Materials Science & Technology 29(10): 909-914

Maijenburg AW, Zoontjes MG, Mul G (2017) Insight into the origin of the limited activity and stability of p-Cu_2O films in photoelectrochemical proton reduction. Electrochimica Acta 245: 259-267

Malachesky PA (1969) Correlation of linear sweep voltammetric and chronoamperometric data for n-value determinations. Analytical Chemistry 41: 1493-1494

Mallick P, Sahu S (2012) Structure, microstructure and optical absorption analysis of CuO nanoparticles synthesized by sol-gel route. Nanoscience and Nanotechnology 2(3): 71-74

Martínez-Ruiz A, Moreno MG, Takeuchi N (2003) First principles calculations of the electronic properties of bulk Cu_2O, clean and doped with Ag, Ni, and Zn. Solid state sciences 5(2): 291-295

Memming R (2001) Electron Transfer Theories. Semiconductor Electrochemistry, 2nd Edition, 127-168

Minami T, Tanaka H, Shimakawa T, Miyata T, Sato H (2004) High-efficiency oxide heterojunction solar cells using Cu_2O sheets. Japanese journal of applied physics 43(7A): L917-L918

Moore DF, Ding Y, Wang ZL (2004) Crystal orientation-ordered ZnS nanowire bundles. Journal of the American Chemical Society 126(44): 14372-14373

Oku T, Yamada T, Fujimoto K, Akiyama T (2014) Microstructures and photovoltaic properties of Zn (Al) O/Cu_2O-based solar cells prepared by spin-coating and electrodeposition. Coatings 4(2): 203-213

Paulonis DF, Oblak JM, Duvall DS (1969) Precipitation In Nickel-Base Alloy 718. Pratt and Whitney Aircraft, Middletown, Conn

Pierson JF, Thobor-Keck A, Billard A (2003) Cuprite, paramelaconite and tenorite films deposited by reactive magnetron sputtering. Applied surface science 210(3): 359-367

Pillai SO (2010) Solid State Physics, New Age International Publishers Revised 6th edition, Chapter 10, pp521

Pleskov YV, Gurevich YY (1986) Semiconductor photoelectrochemistry

Rahdar A, Aliahmad M, Azizi Y (2014) Synthesis of Cu Doped NiO nanoparticles by chemical method. Journal of Nanostructures 4(2): 145-152

Ranu BC, Dey R, Chatterjee T, Ahammed S (2012) Copper Nanoparticle-Catalyzed Carbon Heteroatom Bond Formation with a Greener Perspective. ChemSusChem 5(1): 22-44

Salavati-Niasari M, Davar F (2009) Synthesis of copper and copper (I) oxide nanoparticles by thermal decomposition of a new precursor. Materials Letters 63(3): 441-443

Schroder DK (2006) Semiconductor material and device characterization. John Wiley & Sons

Sharma MK, Qi D, Buchner RD, Scharmach WJ, Papavassiliou V, Swihart MT (2014) Flame-driven Aerosol Synthesis of Copper–Nickel Nanopowders and Conductive Nanoparticle Films. ACS applied materials & interfaces 6(16): 13542-13551

She Y, Zheng Q, Li L, Zhan Y, Chen C, Zheng Y, Lin X (2009) Rare earth oxide modified CuO/CeO_2 catalysts for the water–gas shift reaction. International Journal of Hydrogen Energy 34(21): 8929-8936

Shooshtari L, Mohammadpour R, Zad AI (2016) Enhanced photoelectrochemical processes by interface engineering, using Cu_2O nanorods. Materials Letters 163: 81-84

Shyamal S, Hajra P, Mandal H, Singh JK, Satpati AK, Pande S, Bhattacharya C (2015) Effect of substrates on the photoelectrochemical reduction of water over cathodically electrodeposited p-type Cu_2O thin films. ACS applied materials & interfaces 7(33): 18344-18352

Sieberer M, Redinger J, Mohn P (2007) Electronic and magnetic structure of cuprous oxide Cu_2O doped with Mn, Fe, Co, and Ni: A density-functional theory study. Physical Review B 75(3): 035203

Skoog DA, Holler FJ, Nieman TA (1998) Principles of Instrumental Analysis, Edition Harbor Drive, part IV, Orlando, Florida

Soga T (2006) Fundamentals of solar cell. Nanostructured Materials for Solar Energy Conversion 1: 3-43

Son DI, You CH, Kim TW (2009) Structural, optical, and electronic properties of colloidal CuO nanoparticles formed by using a colloid-thermal synthesis process. Applied Surface Science 255(21): 8794-8797

Stadtländer CTKH (2007) Scanning electron microscopy and transmission electron microscopy of mollicutes: challenges and opportunities. Modern research and educational topics in microscopy 1: 122-131

Štengl V, Bludska J, Opluštil F, Němec T (2011) Mesoporous titanium–manganese dioxide for sulphur mustard and soman decontamination. Materials Research Bulletin 46(11): 2050-2056

Tang Z, Kotov NA, Giersig M (2002) Spontaneous organization of single CdTe nanoparticles into luminescent nanowires. Science 297(5579): 237-240

URL-1,http://www.bayar.edu.tr/besergil/eak_2_1_referans.pdf (date of access: 2017)

URL-2,http://akademi.itu.edu.tr/dokenb/DosyaGetir/58255/ANL1.pdf (date of access: 2017)

URL-3,abs.mehmetakif.edu.tr/upload/1127_904_dosya.pdf (date of access: 2017)

URL-4, http://www.uksaf.org/tech/edx.html (date of access: 2017)

Vijaya Kumar R, Elgamiel R, Diamant Y, Gedanken A, Norwig J (2001) Sonochemical preparation and characterization of nanocrystalline copper oxide embedded in poly (vinyl alcohol) and its effect on crystal growth of copper oxide. Langmuir 17(5): 1406-1410

Wang RY, Jia DZ, Zhang L, Liu L, Guo ZP, Li BQ, Wang JX (2006) Rapid Synthesis of Amino Acid Polyoxometalate Nanotubes by One-Step Solid- State Chemical Reaction at Room Temperature, Advanced Functional Materials 16: 687–692

Weinberg NL (1972) Simplified Construction of Electrochemical Cells. Journal of Chemistry Education 49: 120-121

Wick R, Tilley SD (2015) Photovoltaic and photoelectrochemical solar energy conversion with Cu_2O. The Journal of Physical Chemistry C 119(47): 26243-26257

Wijesooriyage WD (2011) Electrochemical Deposition and Characterization of Thermoelectric Thin Films of $(Bi_xSb_{1-x})_2Te_3$. Chalmers University of Technology

Wiley B, Herricks T, Sun Y, Xia Y (2004) Polyol synthesis of silver nanoparticles: use of chloride and oxygen to promote the formation of single-crystal, truncated cubes and tetrahedrons. Nano Letters 4(9): 1733-1739

Wold A, Post B, Banks E (1957) Rare earth nickel oxides. Journal of the American Chemical Society 79(18): 4911-4913

Xia Y, Yang P, Sun Y, Wu Y, Mayers B, Gates B, Yan H (2003) One-dimensional nanostructures: synthesis, characterization, and applications. Advanced materials 15(5): 353-389

Xu XJ, Fei GT, Yu WH, Wang XW, Chen L, Zhang LD (2005) Preparation and formation mechanism of ZnS semiconductor nanowires made by the electrochemical deposition method. Nanotechnology 17: 426-427

Xue J, Yang H, Shao M, Shen Q, Liu X, Jia H (2017) The influence of Au nuclei layer on formation and photoelectrochemical properties of Cu_2O thin films. Journal of Materials Science: Materials in Electronics 28(12): 8579-8587

Yang P, Yan R, Fardy M (2010) Semiconductor nanowire: what's next?. Nano Letters 10(5): 1529-1536

Yang Y, Han J, Ning X, Su J, Shi J, Cao W, Xu W (2016) Photoelectrochemical stability improvement of cuprous oxide (Cu_2O) thin films in aqueous solution. International Journal of Energy Research 40(1): 112-123

Yang Y, Xu D, Wu Q, Diao P (2016) Cu_2O/CuO bilayered composite as a high-efficiency photocathode for photoelectrochemical hydrogen evolution reaction. Scientific Reports 6: 351-58

Yu SH, Shu L, Yang J, Tang KB, Xie Y, Qian YT, Zhang YH (1998) Benzene-thermal synthesis and optical properties of CdS nanocrystalline. Nanostructured Materials 10(8): 1307-1316

Zhang J, Liu J, Peng Q, Wang X, Li Y (2006) Nearly monodisperse Cu_2O and CuO nanospheres: preparation and applications for sensitive gas sensors. Chemistry of Materials 18(4): 867-871

Zhang S, She G, Mu L, Shi W (2017) A facile fabrication of high-quality Si/Cu_2O nanowire arrays for photoelectrochemical water splitting. Materials Letters 197: 131-134

Zhang Y, Wang S, Li X, Chen L, Qian Y, Zhang Z (2006) CuO shuttle-like nanocrystals synthesized by oriented attachment. Journal of Crystal Growth 291(1): 196-201

Zheng XG, Xu CN, Tomokiyo Y, Tanaka E, Yamada H, Soejima Y (2000) Observation of charge stripes in cupric oxide. Physical Review Letters 85(24): 5170-5171

Zhou Y, Switzer JA (1998) Electrochemical deposition and microstructure of copper (I) oxide films. Scripta Materialia 38(11): 1731-1738

Zhu JJ, Xu S, Wang H, Zhu JM, Chen HY (2003) Sonochemical Synthesis of CdSe Hollow Spherical Assemblies Via an In-Situ Template Route. Advanced Materials 15(2): 156-159

Zoolfakar AS, Rani RA, Morfa AJ, O'Mullane AP, Kalantar-Zadeh K (2014) Nanostructured copper oxide semiconductors: a perspective on materials, synthesis methods and applications. Journal of Materials Chemistry C 2(27): 5247-5270

CURRICULUM VITAE

I was born on January the 1st,1978 in Koya district in Hawler province in which I completed my primary and secondary and high school in there in 1997. I started my bachelor degree in chemistry at Salahaddin University and graduated in 2001. From 2001 to 2016 I worked as a teacher of chemistry in different secondary and high school in Hawler and from 2016 to 2018 I have been pursuing my higher studies at Bingöl University in Turkey and been awarded a master degree in analytical chemistry.